Numerical Investigation of the Mechanical Behaviour of Anastomotic Regions in Vascular Grafts

by

Michael Schaefer

Submitted to the Department of Mechanical Engineering
in partial fulfillment of the requirements for the degree of

Bachelor of Science in Mechanical Engineering

at the

University of Cape Town

October 2006

Advisors: Professor B. D. Reddy and Dr. T. Franz

Declaration

1. I know that plagiarism is wrong. Plagiarism is to use another's work and pretend that it is one's own.

2. I have used the IEEE convention for citation and referencing. Each significant contribution to, and quotation in, this report from the work(s) of other people has been attributed, and has been cited and referenced.

3. This report is my own work.

4. I have not allowed, and will not allow anyone to copy my work with the intention of passing it off as his or her own work.

Signature.....

31^{st} of October 2006

Abstract

Biological or synthetic vascular grafts are commonly used to substitute diseased or damaged tissue. Many potentially life-threatening disorders are remedied by the insertion of vascular grafts. However, with the insertion of these grafts come many potential problems. The areas at which the artificial "veins" are attached to the native biological tissue are particularly vulnerable to complications. Intimal Hyperplasia (IH) is the main cause of thrombotic complications occurring between the second and 24^{th} month after the implementation of a vascular graft [1]. Considerable research has been done to try and understand the causes of IH. Mismatches in the mechanical properties between the graft and the vessel as well as injuries inflicted upon the native vessel as a result of physical handling, have been proposed as major contributing factors. The design of the vascular graft material is crucial to reduce the mismatches in mechanical properties. The process of suturing (stitching) the graft to the vessel is where the vessel is damaged, so the suturing technique is critical too.

The goal of this thesis is to study the effects of compliance mismatches and suturing techniques with particular emphasis on the location and magnitude of stress concentrations.

Acknowledgments

I have enjoyed this project immensely and have learnt a great deal while working on it. I would like to thank my supervisors, Professor Daya Reddy and Doctor Tom Franz, for initiating the project and for guiding my work throughout. This project would not have been possible without their help. I would also like to express my gratitude to the CERECAM, as this work builds on work that has been done there in the past. Sincere thanks to Prof. Reddy, for his suggestions, constructive criticism and boundless patience. In attempting to model the work at the CVRU, Dr. Franz was particularly helpful in providing information on techniques and materials in use. A further thanks to Dr. Franz for organising for me to witness open heart surgery on one of the test baboons. The smell of burning baboon flesh will always be with me (and my clothes)!

Contents

List of Figures

List of Tables

Glossary[1]

Anastomosis The surgical connection of separate or severed tubular hollow organs to form a continuous channel, as between two parts of the intestine.

Anisotropic Having different properties in different directions.

Arteriosclerosis A chronic disease in which thickening, hardening, and loss of elasticity of the arterial walls result in impaired blood circulation. It develops with ageing, and in hypertension, diabetes, hyperlipidemia, and other conditions.

Atherosclerotic A form of arteriosclerosis characterized by the deposition of atheromatous plaques containing cholesterol and lipids on the innermost layer of the walls of large and medium-sized arteries.

Carotid Either of the two major arteries, one on each side of the neck, that carry blood to the head.

CERECAM Centre for Research in Computational and Applied Mechanics.

Compliance The percentage diameter or volume change of a blood vessel per unit increase in internal pressure.

Constitutive Making a thing what it is; essential.

Coronary Of, relating to, blood vessels surrounding the heart.

CVRU Cardiovascular Research Unit, University of Cape Town.

[1]Definitions were obtained from various sources [11, 12, 13, 8]

Diastolic The phase of the heart's pumping cycle during which blood is forced out of the heart.

Distal Anatomically located far from a point of reference, such as an origin or a point of attachment.

Distensability Flexibility

Elastoplastic Having elastic and plastic properties.

Endarterectomy Surgical excision of the inner lining of an artery that is clogged with atherosclerotic build-up.

End to End Configuration of sections such that the end of one section is joined to the end of the other.

End to Side Configuration of sections such that the end of one section is joined to the side of the other.

ePTFE Expanded PTFE

FEM Finite Element Methods.

Femoral Of, relating to, or located in the thigh or femur.

Fibrin Insoluble protein in blood, causing coagulation.

Histology Branch of biology concerned with the structure of organic tissues.

Hyperelastic Non-linear elastic.

Hyperplasia An abnormal increase in the number of cells in an organ or a tissue with consequent enlargement.

Hyperviscoelastic Hyperelastic, but incorporating viscoelastic losses.

Hysteresis The phenomenon exhibited by a system, often an imperfectly elastic material, in which the reaction of the system to changes is dependent upon its past reactions to change.

In vitro In an artificial environment outside the living organism.

In vivo Within a living organism: metabolic studies conducted in vivo; in vivo techniques.

Iliac The uppermost and widest of the three bones constituting either of the lateral halves of the pelvis.

Intima The innermost membrane of an organ or part, especially the inner lining of a lymphatic vessel, an artery, or a vein.

Isotropic Identical in all directions; invariant with respect to direction.

Orthotropic Tending to grow or form along a vertical axis.

Patencies The state or quality of being open, expanded, or unblocked.

Pathological Of the science of disease.

Percutaneous Transluminal Angioplasty (PTA) A procedure for enlarging a narrowed arterial lumen by peripheral introduction of a balloon-tip catheter followed by dilation of the lumen as the inflated catheter tip is withdrawn.

Phenomenological A philosophy or method of inquiry based on the premise that reality consists of objects and events as they are perceived or understood in human consciousness and not of anything independent of human consciousness.

Proximal Nearer to a point of reference such as an origin, a point of attachment, or the mid-line of the body.

PTFE Polytetraflouroethelene.

Stenosis - A constriction or narrowing of a duct or passage; a stricture.

Suture A slender thread, rod, or catheter inserted into a tubular structure, such as a blood vessel, to provide support during or after anastomosis.

Systolic Phase of the heart's cycle during which refilling of the heart takes place.

Thrombosis The formation or presence of a thrombus (a clot of coagulated blood attached at the site of its formation) in a blood vessel.

UHYPER A user defined function written in FORTRAN that defines the behaviour of a hyperelastic material.

Viscoelastic Having viscous as well as elastic properties.

Chapter 1

Introduction

1.1 Project Definition

The junctions (=anastomoses) between native blood vessels and biological or synthetic vascular grafts (blood vessel replacements), are usually critical regions of implants, which if not designed appropriately can limit the performance of the grafts, such as coronary artery bypasses. The main problem is a mismatch between the radial compliance of the native blood vessel and that of the vascular graft. This is caused by a difference in mechanical properties and by the suture used to connect the blood vessel and the implant. Finite element models of several typical blood vessel/graft junctions have been developed to model these interactions.

1.2 Aim of Work

This work aims to carry out a computational study on various techniques used to create anasomoses. Many clinical studies have been and are being conducted in attempts to improve the performances of anatomoses. However, anastomoses *in vivo* are not easily accessible. Even with the creation of *in vitro* models, many difficulties exist in making measurements of mechanical performance. For these reasons, computational models provide valuable insights into the behaviour of areas which cannot be investigated clinically.

1.3 Specific Objectives

The objective of this work is to model the general behaviour of end-to-end anastomoses, particularly the stress concentrations that are generated under physiological conditions. Different methods and materials are used to make these anasomoses, each offering advantages and disadvantages. Two suturing methods and five different materials are investigated.

1.4 Overview of Dissertation

For readers unfamiliar with the histology and mechanical properties of vascular tissue, a brief biological introduction is provided. It is intended to provide a basic understanding of the overall functioning and structure of arteries which computational models aim to simulate. More detailed descriptions are presented by Rhodin [14] and Silver *et al* [15]. The geometry of various anastomoses is described along with the techniques used to model them. Various methods and materials were investigated - in total, six models were created. Each of these models is described, explained and scrutinized. The materials, synthetic and native, are introduced before the finite element modelling procedure is reviewed. Finally, conclusions and recommendations are made. Although the superiority of one technique over another is still unclear, it is hoped that insight into the performance of anastomoses has been provided for future work.

Chapter 2

Biological Theory

2.1 Introduction

Holzapfel [2] cites the major cause of human mortality in the western world as atherosclerosis. According to Holzapfel, it is believed that mechanical factors may be important in triggering the onset of this disorder. Other disorders that are triggered, or thought to be triggered by mechanical factors, include intimal hyperplasia and thrombosis formation. In order for meaningful studies to be conducted, the underlying structure and behaviour of veins and arteries must be understood.

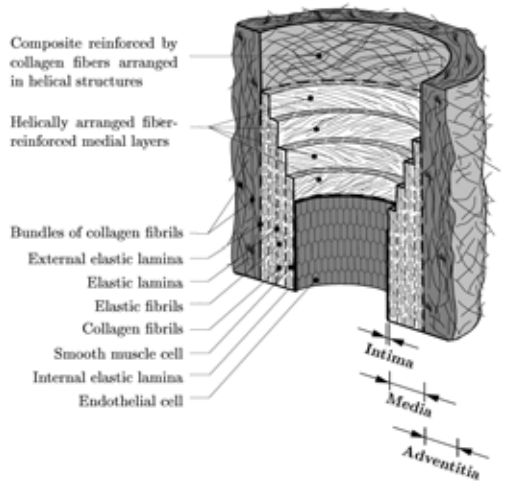

Figure 2.1: General Histology of the Artery [2]

2.2 Histology

Arteries consist of three distinct layers. In order from the inside, the following layers are found: the tunica intima (intima), the tunica media (media) and the tunica externa (adventitia).

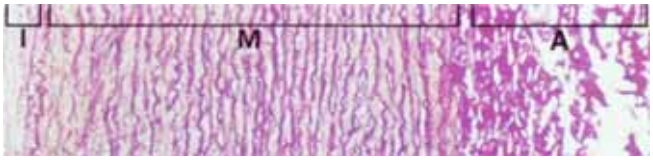

Figure 2.2: Three Layers of Arteries
Intima (I), Media (M) and Adventitia (A) [16]

In healthy young arteries, only the two outer layers, the media and adventitia make solid-mechanically relevant contributions. However, as arteries age, the intima thickens and stiffens (arteriosclerosis), making its contribution significant [2]. The most common disease of arterial walls is atherosclerosis, which involves the deposition of a substance collectively referred to as atherosclerotic plaque. The complex distribution of this plaque, leads to non-homogeneous material behaviour, and difficulty in creating a material model for the plaque. For these reasons, healthy young arteries in which the intima does not make solid-mechanical contributions were modelled. As described in chapter 7, "Finite Element Methods", only the media and the adventitia were modelled in this study.

The most mechanically significant layer in healthy young arteries is the media. This layer consists of a complex three-dimensional network of smooth muscle cells and elastin and collagen fibrils. Together, these constituents form a fibrous helix, with the fibrils arranged with a very small helical angle, giving the structure great strength in the longitudinal and circumferential directions. These fibres are one of the main sources of the anisotropic, non-linear elastic behaviour of arteries, discussed below in chapter 2.5, "Mechanical Properties of Arteries".

The outermost layer, the adventitia, also contains connective tissue arranged in a helical structure. The media is much stiffer than the adventitia under low pressure. However, at higher pressure, when the connective tissue in

the adventitia is put into tension, it becomes very stiff, forming a rigid casing around the artery. This protects the artery from over-stretching and rupturing [2].

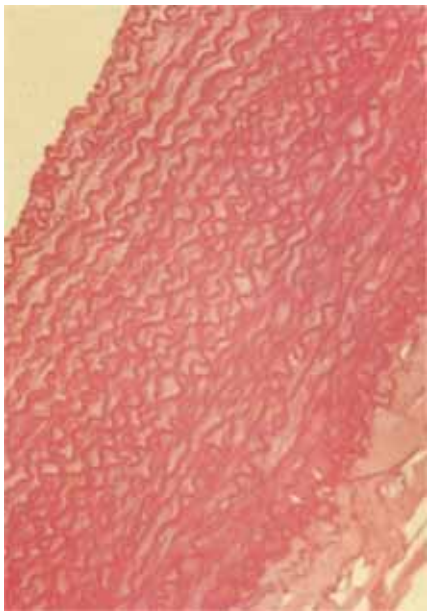

Figure 2.3: Elastic Fibres within Arteries [3]

2.3 Artery Diseases and Causes

Lemson *et al* [1] cite the main cause of thrombotic complications occurring between the second and 24^{th} month after the implementation of a vascular graft as Intimal Hyperplasia (IH). Lemson *et al* [1] give an in-depth description of the mechanisms of Intimal Hyperplasia in their paper "Intimal Hyperplasia in Vascular Grafts". Considerable research has been done to try and understand the causes of IH. Mismatches in the mechanical properties between the graft and the vessel, the compliances in particular, the incompatibility of the biomaterials, as well as injuries inflicted upon the native vessel as a result of physical handling, have been proposed as major contributing factors. The design of the vascular graft material is crucial to reduce the mismatches in mechanical properties. The process of suturing (stitching) the graft to the vessel is where the vessel is damaged, so the suturing technique

is critical too. The suturing technique also influences the compliance matching between the native and synthetic sections. The various techniques are discussed in chapter 3, "Anastomosis Geometry".

Arteries can adapt their diameter to maintain a relatively constant wall shear stress [17]. This is facilitated by a range of vasoactive agents that are secreted by the cells lining the inside of arteries. Synthetic sections cannot do this. The sizing of the graft therefore becomes crucial, as it cannot vary. The pressure at which the sizes are matched is also vital, considering the different compliances of different materials. Weston *et al* [18] did an in-depth study into the sizing of grafts and they proposed that the optimal size was 6 % smaller than the native artery, at physiological pressure. However, this depends on the graft and artery materials.

As mentioned above, the wall shear stress (and also the gradient thereof) in arteries is widely believed to be a factor in the formation of Intimal Hyperplasia. The shear stress on the wall is governed by the fluid dynamics (haemodynamics) of a particular region. An investigation of these influences is beyond the scope of this work.

2.4 Arterial Tree

The mechanical properties of arteries are not constant throughout the arterial tree. Arteries found close to the heart are subjected to the highest pressure (about 100mmHg [19]) and are responsible for smoothing and damping the pulsatile flow generated by the heart. They dilate during the systolic phase (contracting, forcing phase) to absorb the sudden rush of blood and contract during the diastolic phase (refilling phase) to maintain blood flow and pressure. Noble *et al* [19] explain that the role of the heart is "to keep the arterial pressure reserve 'topped up"'. The most pulsatile flow is hence found close to the heart. Arteries with the highest compliance are thus situated close to the heart and compliance decreases steadily as one moves further from the heart. Milnor [20] states that the elastin (flexible) to collagen (rigid) ratio changes from 2 in the aortic arch to 0.5 in the abdominal aorta. This is reinforced by Shadwick's [21] observation that the ratio of the flow pulse amplitude to the mean flow decreases from about 6 in the aortic arch to less than 2 in the

femoral artery.

2.5 Mechanical Properties of Arteries

The mechanical properties of arteries vary considerably from patient to patient. This is because factors such as age, fitness, temperature, pH and ionic concentration, to mention but a few, vary between individuals. That said, arteries generally have the following characteristics in common.

Shadwick [21] cites the most important mechanical property of the artery as its non-linear elasticity. According to him, this has been well documented in vessels in many animals, from humans to lobsters. As described above, arteries smooth the pulses generated by the heart and perform a capacitive role too. In order to meet these requirements, the vascular walls have a strain dependent elastic modulus, with the greatest compliance coinciding with the normal blood pressure range. The J-shaped stress-strain curve below illustrates this.

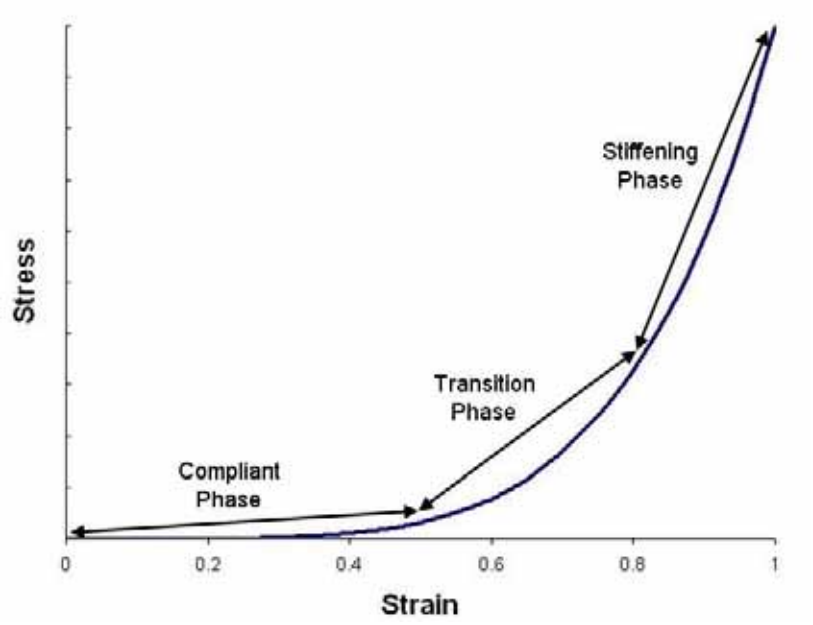

Figure 2.4: J-Shaped Stress Strain Curve

Owing to the multi-layered composite structure of vascular walls, their behaviour is not only non-linear elastic, but also anisotropic. The collagen fibrils that are found within the media and adventitia are much stiffer than the elastin matrix. Shadwick [21] claims that the elastin has an elastic modulus of 1 MPa compared to 1 GPa for the collagen. However, the collagen fibrils are arranged concentrically around the circumference of the vascular walls at an angle. The structure is therefore compliant at low pressures but very stiff at higher pressures when the collagen fibrils are aligned and put into tension. This allows for expansion at low pressures, while preventing overstretching and rupture at higher pressures. These properties are included in the material model that was developed by Saleeb *et al* [22].

A further complexity in the behaviour of arteries is the presence of viscoelasticity with an associated hysteresis loop. Shadwick [21] explains the phenomenon as follows: "When an artery is subjected to inflation-deflation cycles, viscoelasticity will cause the pressure-volume curve for deflation to fall below that for inflation, forming a hysteresis loop. The area enclosed by this loop represents the energy lost in each cycle which, for most arteries, is of the order of 15-20 % of the total strain energy input. This means that most, but not all, of the strain energy is recovered elastically each time the artery wall is distended". According to Fung [23], the strain energy lost by viscoelasticity helps to attenuate travelling pressure pulses, which propagate along arteries as waves of circumferential distention of the vessel wall. In combination with the viscosity of blood, this phenomenon prevents reflected pressure waves from resonating in the arterial system, as it would if arteries were perfectly elastic and blood was inviscid. This phenomenon is a complex one to model mathematically, but the model proposed by Saleeb does so.

According to Delfino *et al* [24], "Several studies have demonstrated that the introduction of residual stress on the artery model is important for accurate calculation of the stress distribution throughout the wall thickness of the artery". Holzapfel *et al* [2] is in agreement, incorporating the residual stresses of arteries into his work.

Arteries in an unloaded state are not stress-free. This can be shown by cutting an artery longitudinally. Once cut, the artery will spring open to form an open sector. The angle included by the sector is given by Delfino et

al as 130°. This is based on the measurement of eight human carotid arteries with a standard deviation of 15°. Holzapfel uses an included angle of 100°. As described later, the pre-stress in arteries was included in the finite element modelling.

Not only are arteries pre-stressed in a circumferential direction, but also axially. Delfino *et al* [24] measured the axial stretches of human carotid arteries in situ and gives the average stretch as 10 %. Holzapfel *et al* [2] use this value in their work too, although Schajer *et al*[25] claim that arteries are typically stretched longitudinally by between 30 and 60 %, depending on the location of the artery and the health and age of the patient. This is consistent with the elastic property data presented by Fung *et al* [26]. Longitudinal pre-stress was included in the finite element models.

Chapter 3

Anastomosis Geometry

3.1 Introduction

There are three geometrical configurations for the creation of anastomoses: End-to-end, end-to-side and side-to-side. To go along with each of these configurations, there are two suturing techniques, as described below.

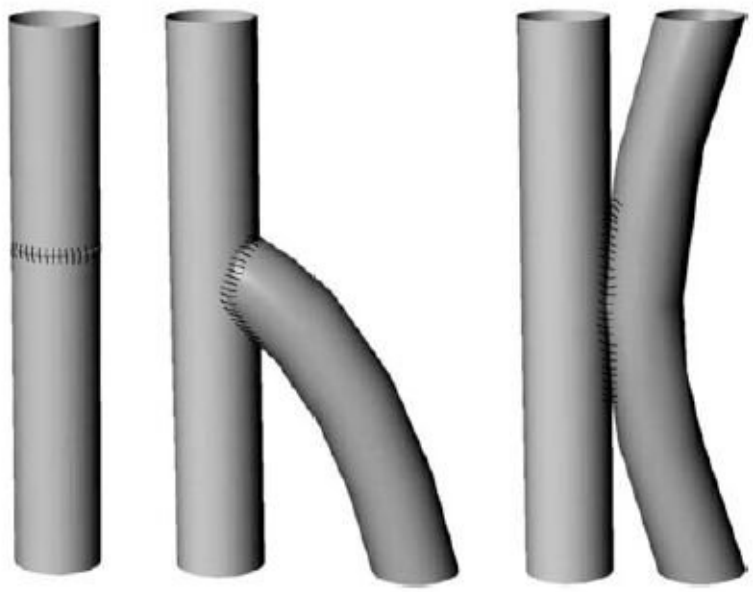

Figure 3.1: From left: End to end, End to Side and Side to Side Anastomoses [4]

3.2 Stitching Patterns and Techniques

There are many ways of forming an anastomosis. Biological glues, clips, laser generated solders [27] and stitches are among the many methods. However, the most used method, the method investigated in this work, is the stitching method. In particular, the anastomosis investigated is the end-to-end anastomosis. Figure 3.2 below shows a femoral artery interposition graft in one of the test baboons from the CVRU. In this case, the graft is vascular, sourced from the femoral vein of the baboon.

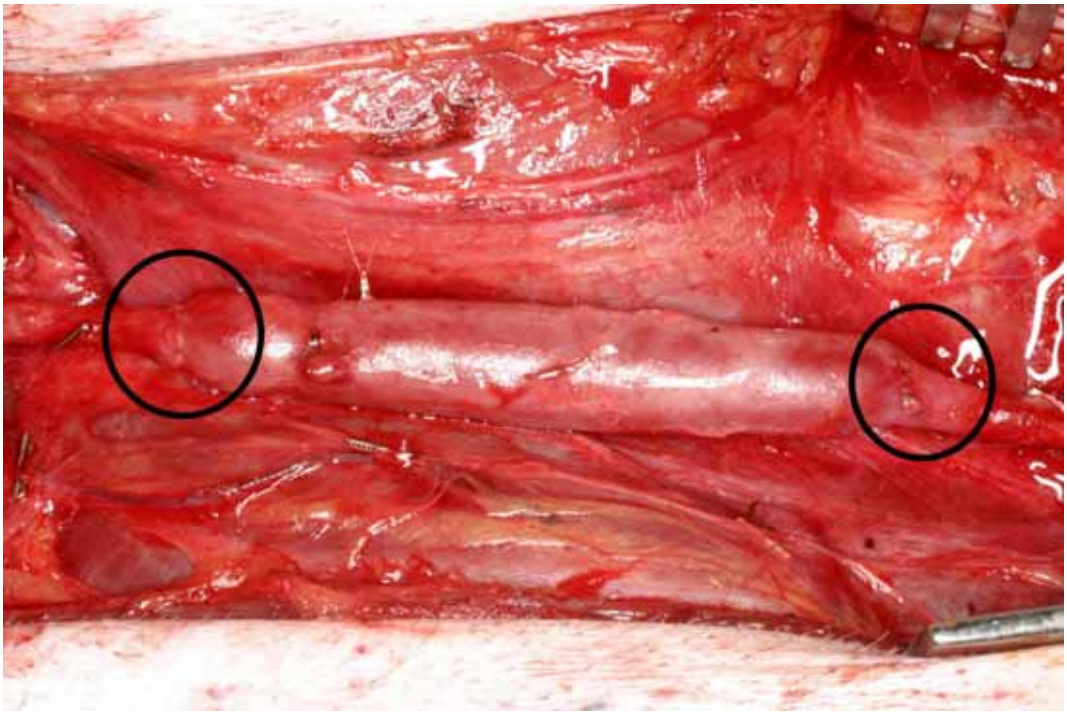

Figure 3.2: Femoral Graft Courtesy of the CVRU
Note that the graft has the larger diameter

3.2.1 Suturing Patterns

There are two commonly used suturing patterns. The first, continuous suturing, utilises a single length of suturing material to weave between the two sections. The second, interrupted suturing, employs multiple tied-off stitches to connect the sections. The advantage of the continuous technique is its ease of implementation. The surgeon only needs to use one length of suture, starting only once and ending only once. This saves time and reduces the handling of the tissue, lessening the risk of bleeding from suture lines [27].

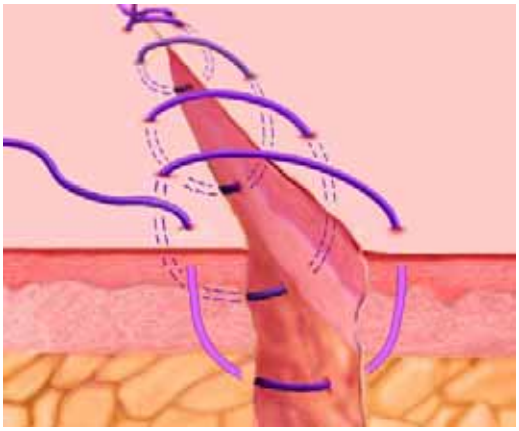

Figure 3.3: Continuous Stitching [5]

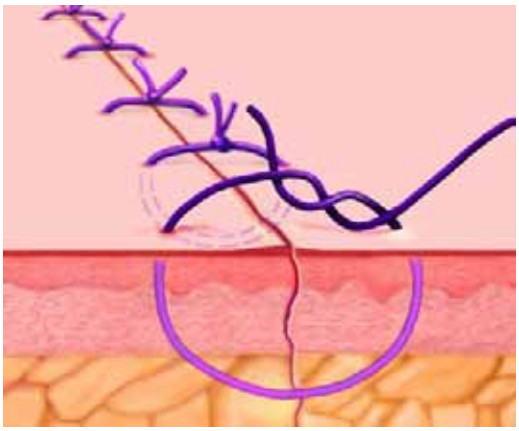

Figure 3.4: Interrupted Stitching [6]

A further problem is the potential formation of a "purse-string" effect which, according to Tiwari, impairs the haemodynamic effect at the anastomosis. The continuous technique forms diagonal connections between the sections, reducing the compliance of the anastomosis - one of the major causes of arterial disease and graft failure.

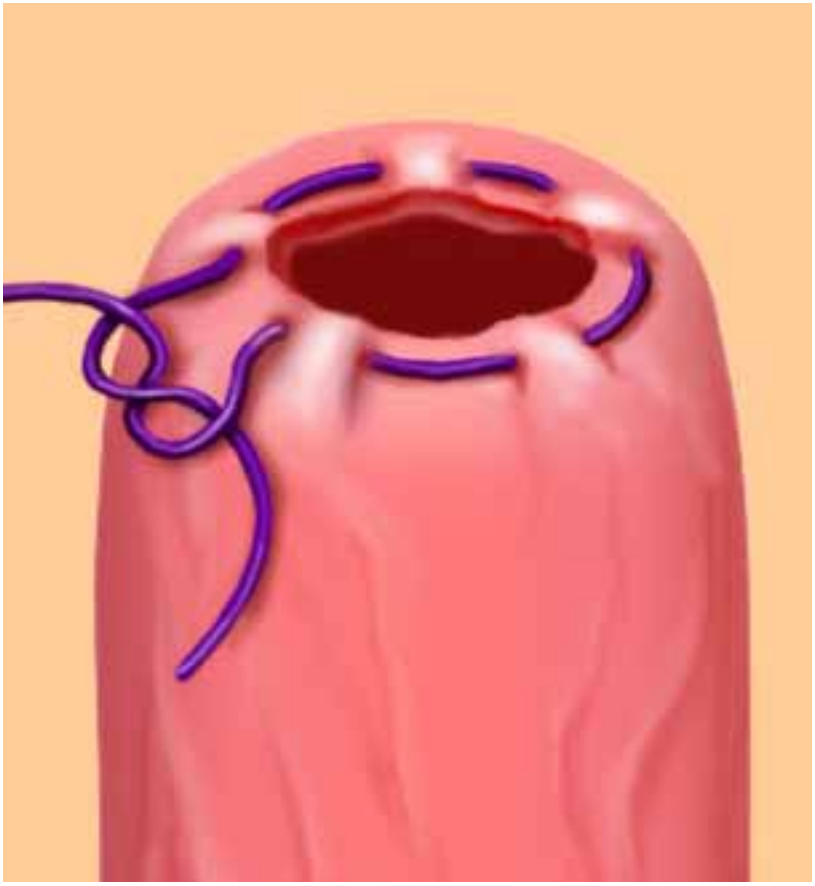

Figure 3.5: Purse String Effect [7]

This contrasts with the interrupted technique, which requires a start and an ending for each "loop" that is made. The sections are handled more as a result of the greater complexity. However, the primary advantage of interrupted stitches is their minimal impact on the compliance of the anastomosis. Seeing as all the stitches may move independently, the circumferential stiffness of the graft is reduced dramatically.

Chapter 4

Anastomoses Modelled

4.1 Introduction

The various anastomoses modelled in this work are described below. Three different sections were modelled and for each section, the interrupted and continuous stitching patterns are investigated. The modelling assumptions and techniques are elaborated on below.

4.2 Vascular to Vascular

4.2.1 Introduction

The properties of vascular tissue are described in chapter 2.5, "Mechanical Properties of Arteries". In order to model the differing properties of the differing vascular sections (eg. vein onto artery), the constants used in the UHYPER were modified. However, as a control, identical vascular sections were connected using interrupted and continuous stitching. The pre-stressing of the sections was considered to be very important in the successful modelling of this kind of junction. The simulation makes use of several steps to pre-stress the sections, "load" the stitches and apply the pressure pulse.

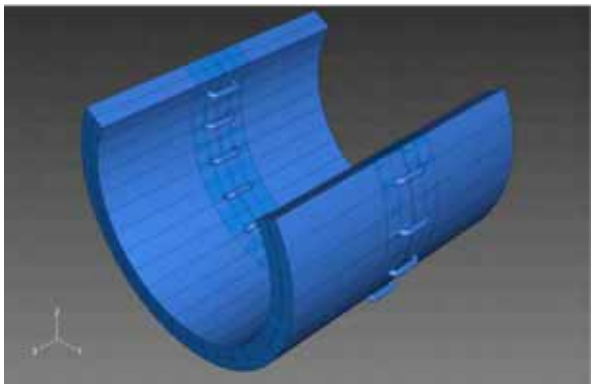

Figure 4.1: Initial Configuration of Vascular to Vascular Anastomosis

4.2.2 Interrupted Stitches

To model interrupted stitches, closed hoops were used to attach the two sections throughout the analysis. During the pre-stressing of the sections, the corresponding holes in the sections moved together, allowing hoops to be used (as opposed to separate U-shaped stitches). To model the interrupted technique, adjacent hoops were not connected in any way, simulating the individual stitches used clinically. The hoops were free to move radially, being constrained in their axial motion.

4.2.3 Continuous Stitches

Similarly to the model of the interrupted stitches, closed hoops were used to model the continuous stitches. However, to model the continuous stitching pattern, axial connectors were used to connect adjacent hoops together. During the analysis, a step was dedicated to the loading of the stitches to create the "purse-string" effect mentioned before.

4.3 Vascular to Synthetic

4.3.1 Introduction

Vascular grafts are preferred to synthetic grafts. However, suitable, healthy native tissue cannot always be sourced from elsewhere in the body, due to disease or simply age. Also, the use of native tissue requires an additional surgical intervention with an additional anastomosis being necessary to repair the site from which the native section was removed. For these reasons, considerable research has been and is being done to develop synthetic grafts with suitable properties.

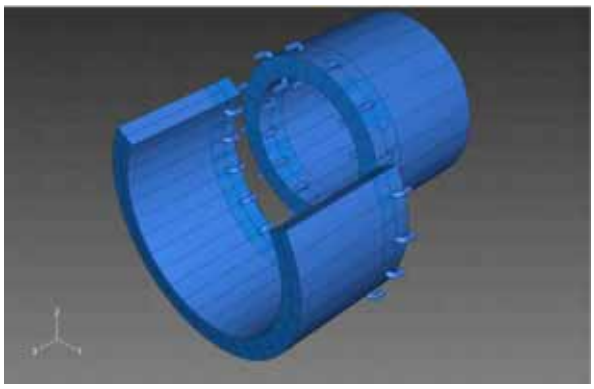

Figure 4.2: Initial Configuration of Vascular to Synthetic Anastomosis

4.3.2 Interrupted Stitches

As in the vascular to vascular model, the vascular portion of this model started the analysis as an open sector which was subsequently bent into a cylinder to simulate the physiological pre-stresses. The synthetic section does not experience the circumferential pre-stress that the native section does. The synthetic section is therefore modelled as a closed cylinder from the outset. These different initial conditions make it impossible to model the stitches with closed loops. In their places, U-shaped stitches are used.

The vascular section is bent into shape (figure 4.3) during the first step, after which its stitches are connected via axial connectors to the stitches in the cylindrical, synthetic section. The interrupted pattern is simulated by

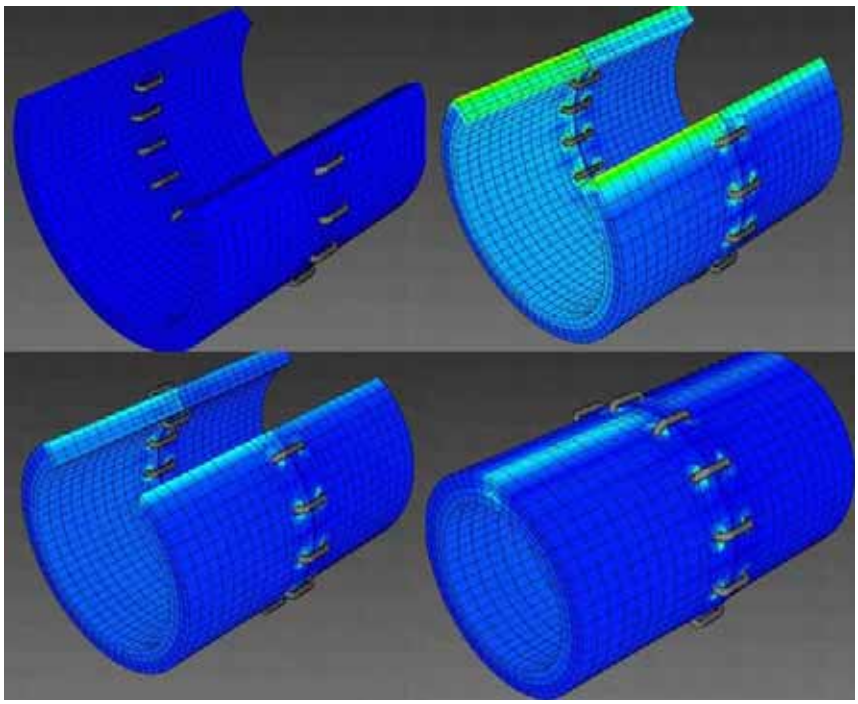

Figure 4.3: Bending and Pre-stressing of Vascular Sections

using either hoop stitches, or by applying contracting loads onto the "axial" connectors joining the sections. See chapter 7.6, "Interactions" for more details.

4.3.3 Continuous Stitches

The same initial conditions are used for this model. The difference between this model and the previous one is in the manner in which the stitches are connected together. To simulate the continuous pattern, "axial" connectors were used in combination with "link" connectors. The "link" connectors were used to join the stitches in the synthetic material, while the "axial" connectors were used to join the stitches in the synthetic and vascular sections. See chapter 7.6.

4.4 Synthetic to Synthetic

4.4.1 Introduction

To illustrate the influence of pre-stressing the arteries before applying loads, this model examines interactions between various sections which are not initially pre-stressed. Not only are the effects of omitting the initial stresses in arteries demonstrated, but the model correctly models the initial state if both sections are synthetic. Due to the fact that this model requires no relative motion between the sections to prepare them for loading, the hoop stitches mentioned before could be employed again.

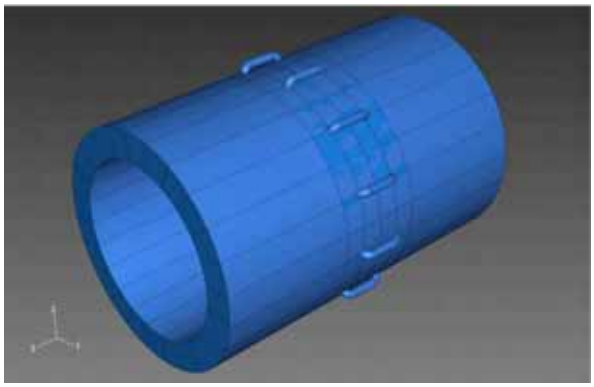

Figure 4.4: Initial Configuration of Synthetic to Synthetic Anastomosis

4.4.2 Interrupted Stitches

Owing to the fact that closed hoops were used in this model, no connectors were required to model the interrupted technique.

4.4.3 Continuous Stitches

As before, axial connectors were used to connect adjacent stitches. A different kind of connector, the "link" connector was also employed on this model. See chapter 7.6.

Chapter 5

Graft Materials

The mechanical properties of the graft, whether synthetic or biological, are crucial to the success of the implant. Many different materials have been tested and utilised as grafts with varying degrees of success. The most common problem is that of a compliance mismatch at the anastomosis. Tiwari *et al* [27] refers to two different kinds of compliance mismatch - tubular and anastomotic. They define tubular compliance as "resistance to pulsatile flow". This kind of mismatch is most problematic at the site of an anastomosis, as this is where two different sections with differing mechanical properties meet. According to Tiwari et al, this compliance mismatch results in only 60 % of the original pulsatile to be propagated past the joint. Anastomostic compliance mismatch is caused by the decrease in diameter and compliance due to the stiffness and "purse-string" effect of the suturing (See figure 3.5). Both of these issues influence prosthetic bypass grafts more than native bypass grafts due to the lower compliance of most synthetic materials compared with native vascular tissue.

Synthetic materials, such as Dacron, Silicone and polytetrafluoroethylene (PTFE) are more rigid than the native vessels. Comparative values at 133kPa are given by Zidi *et al* [28] in table 5.1.

	Young's Modulus (MPa)	Compliance (%/MPa)
Artery	0.455	677
PTFE	2.2	124
Dacron	1.9	145
Silicone	0.498	494

Table 5.1: Compliance and Young's Modulus for Synthetic and Vascular Sections

To compound the problem, the compliance of expanded PTFE (ePTFE) is reduced to 14 percent and Dacron to 29 percent of their pre-implantation levels after 3 months of implantation [27].

A further problem is the matching of diameters. Together, these factors cause shear rate disturbances which may cause intimal hyperplasia, which in turn might lead to graft failure [18].

Biological vascular grafts are often used instead of synthetic ones. In such a procedure, a portion of healthy vascular tissue is sourced from the patient and is then used elsewhere in the body to replace diseased or damaged tissue. However, as is explained in chapter 2.2, "Histology", the mechanical properties of arteries and veins differ considerably throughout the body. Thus, a perfect match is not guaranteed. Another complication is that an extra junction must be made to repair the site from which the sample was taken.

Research at the Cardiovascular Research Unit (CVRU) is currently being done on such grafts. Baboons are used as test subjects. Sections of their saphenous veins (the main vein in the calf) are removed and used to bypass sections of the heart. Also, femoral grafts are inserted. The end-to-end model that was developed attempts to simulate their work. For this reason, the materials, suturing pattern and dimensions are based on their clinical work. The material that is used to simulate the artificial graft was developed, tested and modelled by Yeoman [8] in his PhD thesis. It is made from polyurethane, which is cast into a tubular section. Within the walls

of the tube, small porogens gelatin micro-spheres are implanted while the polyurethane is still malleable. Once set, these small balls are dissolved and removed from the polyurethane, leaving air gaps in the material. This creates a spongy composition. The foam section is lined with a thin layer of latex, which serves to seal the foam. The latex makes no solid mechanically relevant contributions.

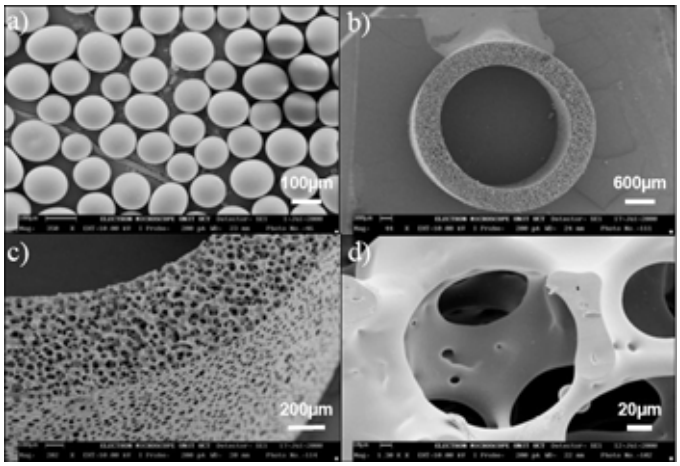

Figure 5.1: Synthetic Material Created by Yeoman [8]

The suturing material that is used is a 0.14mm diameter polypropolene section, with the trade name of *Prolene*®.

Chapter 6

Mathematical Underpinnings of the Material Model

6.1 Introduction

As explained in chapter 2.5, "Biological Theory", the mechanical characteristics of vascular walls are non-linear elastic and anisotropic. In order to realistically model the non-linear behaviour, a strain energy function is required to define the hyperelastic behaviour. Hyperelastic behaviour is characterised by a J-shaped stress-strain curve (the red curve in figure 6.1). Various functions have been developed to model this behaviour, including exponential functions, one of which has been implemented in this work. Although several simplifying assumptions were made in the development of the model, behaviour within the physiological range is closely modelled.

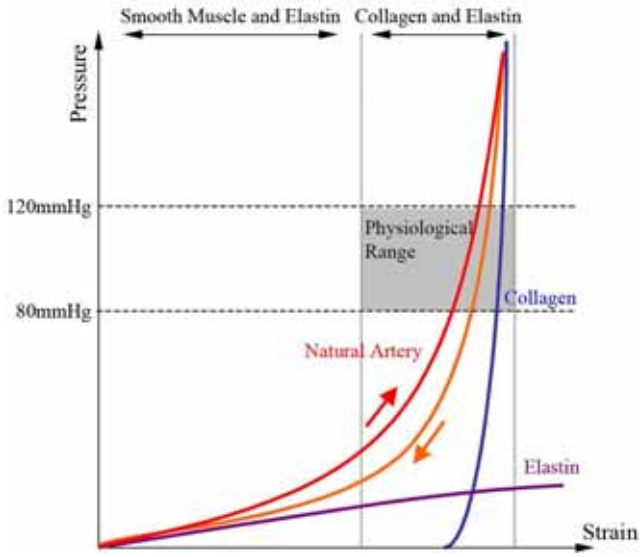

Figure 6.1: The Non-linear Elastic and Viscoelastic Behaviour of Blood Vessel Tissue and the Interaction between Collagen and Elastin. Graph from [8].

6.2 Assumptions of the Implemented Model

Purely hyperelastic materials follow the same curve during the loading and unloading phases. Modelling vascular tissue as purely hyperelastic is an approximation of the actual hyperviscoelastic behaviour of arteries. The orange line in figure 6.1 shows the return path that a viscoelastic material would take. Seeing as the area beneath a stress vs strain curve represents the strain energy in a system, the area between the red and orange line represents the energy dissipated during each cycle. The effects of this are explained in chapter 2.4, "Arterial Tree". During normal physiological activity, the material is almost perfectly elastic, with viscoelastic effects being small. Loading can occur outside of the elastic domain during some surgical procedures, such as Percutaneous Transluminal Angioplasty (PTA). If deformations on such a scale were to be simulated, the modelling of the helical fibrils, the hysteresis loop and the viscoelasticity would be very important. Be that as it may, only activity within the normal physiological operating range is modelled, so the

omission of the above-mentioned factors is deemed acceptable.

6.3 Mathematical Model Implemented

Some strain energy functions are built into $ABAQUS^{®}$, such as the Ogden, Mooney-Rivlin, Neo-Hookean, etc. However, if it is desired to implement a model which is not incorporated into $ABAQUS^{®}$, it is necessary to write a user-defined function, a UHYPER, in FORTRAN.

Based on the work of Delfino *et al* [24], a UHYPER was created and implemented. The strain energy function proposed by Delfino *et al*, incorporates the hyperelastic, non-linear behaviour of vascular walls. The function aims to model thick-walled, incompressible tissues. It does not include the anisotropic behaviour, the viscoelasticity, nor does it make provision for the non-homogeneous nature of tissues.

For the UHYPER, $ABAQUS^{®}$ requires the first and second partial derivatives of an *isotropic* strain energy function with respect to the invariants, $\frac{\partial W}{\partial I_1}$, $\frac{\partial^2 W}{\partial I_1^2}$, etc.
The strain energy function proposed is *isotropic* and W therefore only depends on the invariants and constants:

$$W = \frac{a}{b}\left\{e^{\left\{\frac{b}{2}(I_1-3)\right\}} - 1\right\}$$

where a and b are constants and I_1 is the first invariant, defined by

$$I_1 = trC = \lambda_1^2 + \lambda_2^2 + \lambda_3^2.$$

λ_i is the principal stretch in the ith direction and is given by

$$\lambda_i = \frac{deformed\ length}{original\ length\ of\ a\ fibre\ aligned\ with\ the\ i^{th}\ principal\ direction}$$

and C is the Cauchy-Green deformation tensor.

The partial derivatives then are given by

$$\frac{\partial W}{\partial I_1} = \frac{a}{2}\left\{e^{\left\{\frac{b}{2}(I_1-3)\right\}}\right\} \qquad \text{and} \qquad \frac{\partial W}{\partial I_1^2} = \frac{ab}{4}\left\{e^{\left\{\frac{b}{2}(I_1-3)\right\}}\right\}$$

The material is assumed to be incompressible, so $I_3 = 1$,

where

$$I_3 = detC = \lambda_1^2\lambda_2^2\lambda_3^2$$

The fact that $I_3 = 1$ and that W is function of only the first two invariants, leads to all of the other partial derivatives being equal to zero.
The constants a and b are provided by Delfino *et al* in their paper. The full sub-routine is given in Appendix A, along with the constants. The work of Koch [29] provided an excellent guide to writing this subroutine, along with the $ABAQUS^{®}$ User Manual.

Chapter 7

Finite Element Modelling

7.1 Introduction

All of the models were created in $ABAQUS^{®}$. $ABAQUS^{®}$ is a suite of finite element applications, including $ABAQUS^{®}$\CAE and $ABAQUS^{®}$\Standard. CAE is an interactive environment used to create finite element models, submit $ABAQUS^{®}$ analyses, monitor and diagnose jobs, and evaluate results [9]. Standard is a general-purpose finite element program which accepts jobs submitted from CAE and solves the systems of equations implicitly (establishes equilibrium) in each increment. Standard is suitable for the analyses, as the effects of inertia are negligible and the assumption of a quasi-static procedure is deemed to be acceptable. For more detail on the characteristics of Standard, the reader is referred to the $ABAQUS^{®}$ user manual [9].

7.2 Parts

In order to model the circumferential pre-stress in the artery, an open sector was created. The included angle was 120° - within the range proposed by Delfino *et al* [24] ($130° \pm 15°$). Initially, the sector's outer diameter was 5.7mm, while its internal diameter was 4.7mm. When closed, the internal diameter was 3mm, with the closed outer diameter 4mm. These dimensions were used to match the work at the CVRU. Twelve 0.14mm diameter holes were punched radially through the 0.5mm thick walls. In practice, the num-

ber of stitches varies from one operation to the next, with numbers typically close to 12. Each stitch was modelled as rigid, as the stiffness of the stitches is far greater than that of the surrounding tissue. A stitch was created using discrete rigid shells. Shells were used, as the structure is completely rigid and only the outer surface is relevant (for contact interactions). For some of the final models, it was possible to model the stitch as a closed loop. In such cases, a hoop was formed using discrete rigid shells.

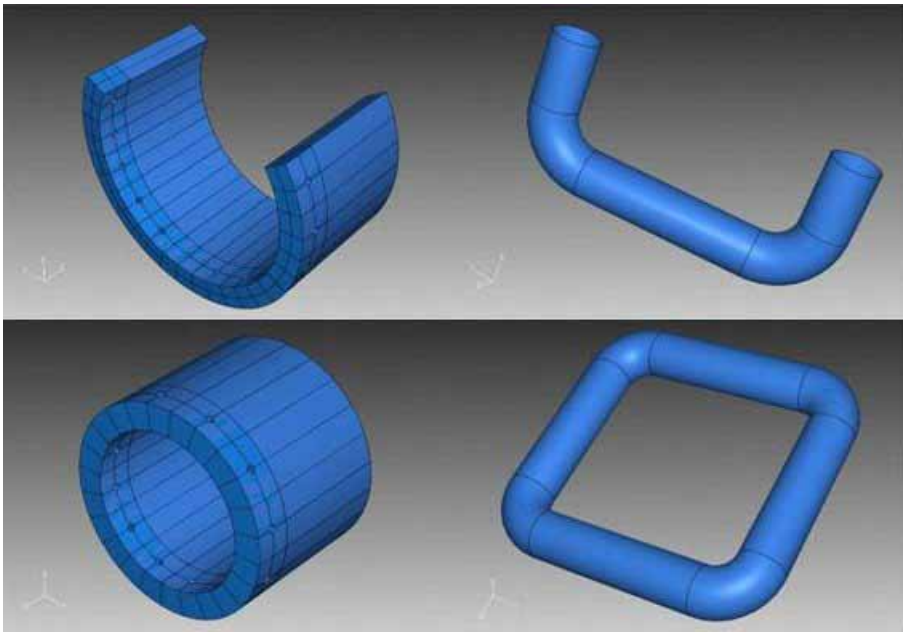

Figure 7.1: Various Parts Used
Clockwise from top left: Vascular, U-Stitch, Hoop and Synthetic

7.3 Properties

As explained in chapter 2, "Biological Theory", there are three distinct layers in arteries, the media, the adventitia and the intima. Recalling that the intima does not make significant solid mechanical contributions to the performance of healthy young tissue, only the media and adventitia were modelled. To model the different layers, a longitudinal partition was created in the vascular section. The layers were assumed to be of a similar thickness, so the total thickness of the artery was bisected by the partition. A different material was then assigned to each partition. See Appendix A for the constants and methodology used.

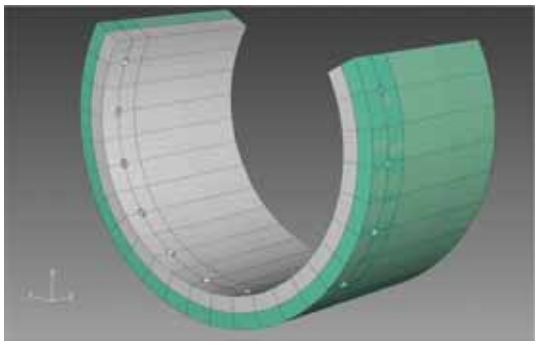

Figure 7.2: Different Properties Assigned to Media and Adventitia

The material that was used to model the grafts was a polyurethane "sponge", as used by the CVRU in some of their experimental work. This material was developed and tested by Yeoman in his PhD Thesis [8](figure 5.1). In his thesis, he gives the material constants for a hyperfoam model in $ABAQUS^{®}$ with n=4. This model was used for the synthetic material.

The stitches required no property definition, as they were modelled as being rigid.

The vascular tissue was modelled using a user-subroutine based on the work of Delfino *et al* [24], see chapter 6, "Mathematical Underpinnings of the Material Model". This was incorporated by specifying an isotropic user-defined strain energy potential. The keywords of the model were then edited to specify the constants required by the subroutine. The sub-routines are given in Appendix A.

7.4 Assembly

The two sections were positioned coaxially, except for the synthetic to vascular simulation. In this case, the cylindrical synthetic section was positioned to align with the closed vascular section. The position of the sector was calculated to align its stitches with those from the cylindrical section.
The same stitch part was used, with a separate instance created for each hole. The stitches were placed through their respective holes before pre-stressing. Although not entirely realistic, the insertion of the stitches before the pre-stressing simplified the analysis enormously and does not yield unrealistic initial conditions. The same behaviour is to be expected if the stitches were inserted after pre-stressing.
In some analyses, the two sections were placed so that they interfered before the pre-stressing of the artery. By doing this, the gap between the sections was minimized under loading.

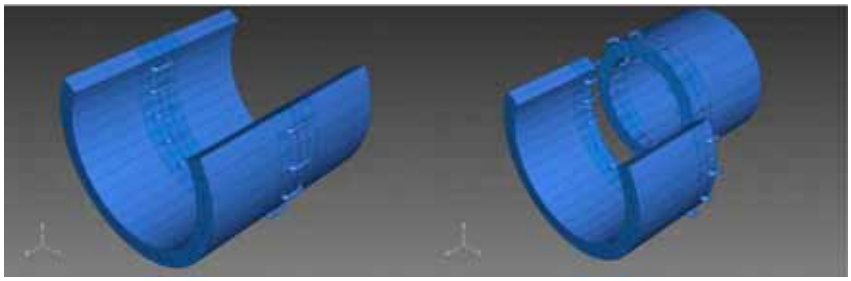

Figure 7.3: Cylinder Section Assembly

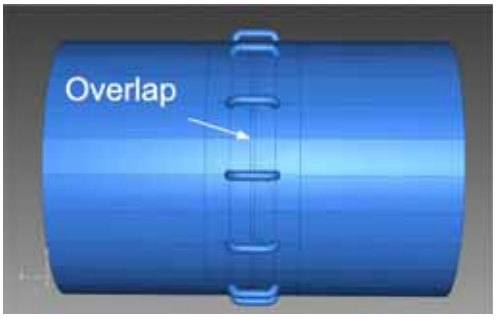

Figure 7.4: Cylinder-Cylinder Assembly Showing Initial Interference

7.5 Step

All of the steps that were used were static-general steps. $ABAQUS^{®}$/Standard was employed for all of the final simulations. The *Nlgeom* feature was implemented in this step to make provision for the non-linear geometrical behaviour that was expected.

Restart requests were enforced for all steps, obviating the repetition of successful steps.

7.6 Interactions

All of the contact interactions between components were modelled as tangential, frictionless interactions. Friction does not play a significant role in the interactions and its omission was viewed as an adequate approximation to reality. To get the simulation to run smoothly, the friction interactions were modelled under the pretence that only small sliding displacements would take place. By small, the displacements were assumed to be a fraction of the size of the elements involved in the interaction. To prevent overclosure, the two surfaces in contact were allowed to be adjusted only enough to prevent overclosure.

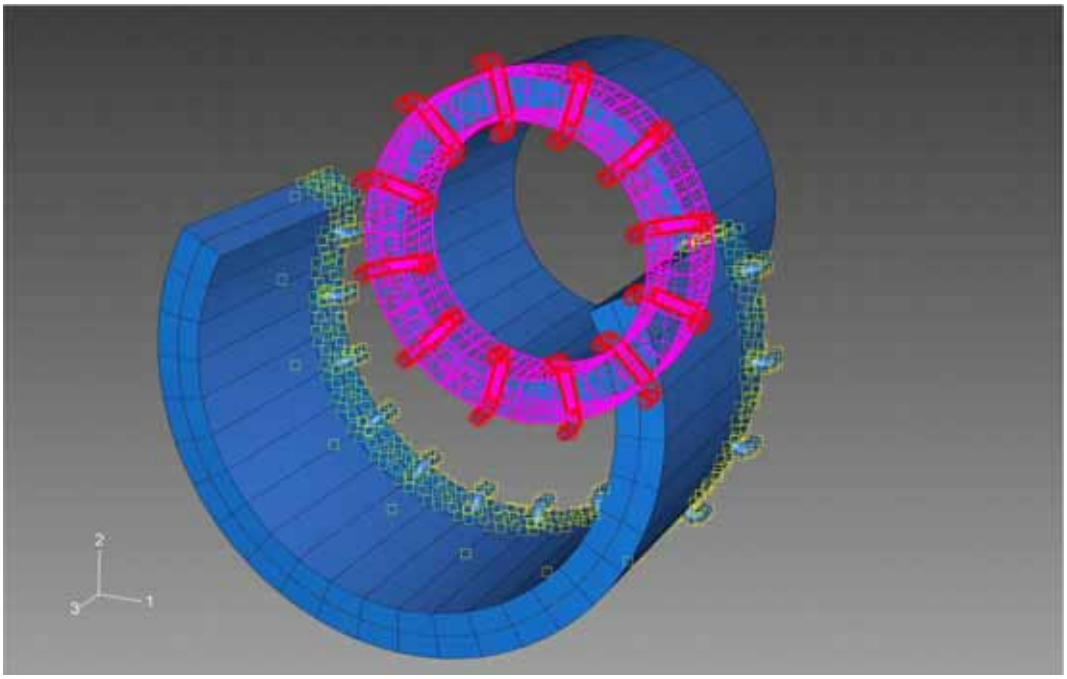

Figure 7.5: Frictional Interaction

Connectors were used to connect the individual stitches together. For some of the analyses (continuous synthetic), it was possible to use "link" connectors, but where that was not possible, "axial" connectors were used.

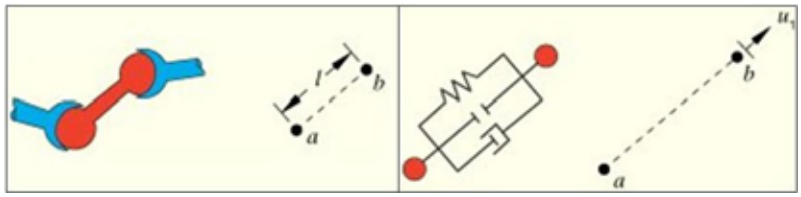

Figure 7.6: Link and Axial Connectors. Image from [9].

"Link" connectors join two points together by maintaining a constant distance between them. It places no restrictions on their motion, other than keeping the magnitude of their separation distances constant.

"Axial" connectors join two points together, but the magnitude of the distance between the points may be varied. No restrictions are placed on the motion of the points, except in the direction of the vector joining the points together. The distance in this direction may be controlled or a force may be exerted in this direction.

In some of the simulations, forces were prescribed along the axial connectors in certain steps, while in others, displacements were prescribed. This was done in order to simulate the tensioning of the stitches due to the surgeon.

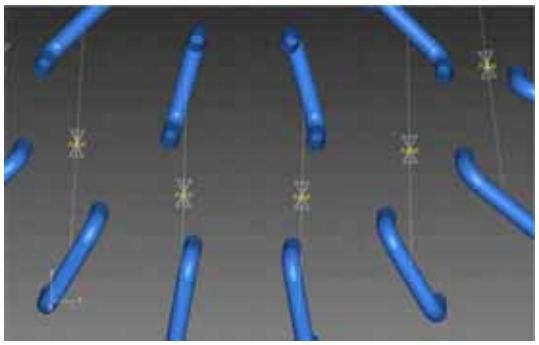

Figure 7.7: Connector Forces

The connection patterns that were utilised are illustrated on the following page.

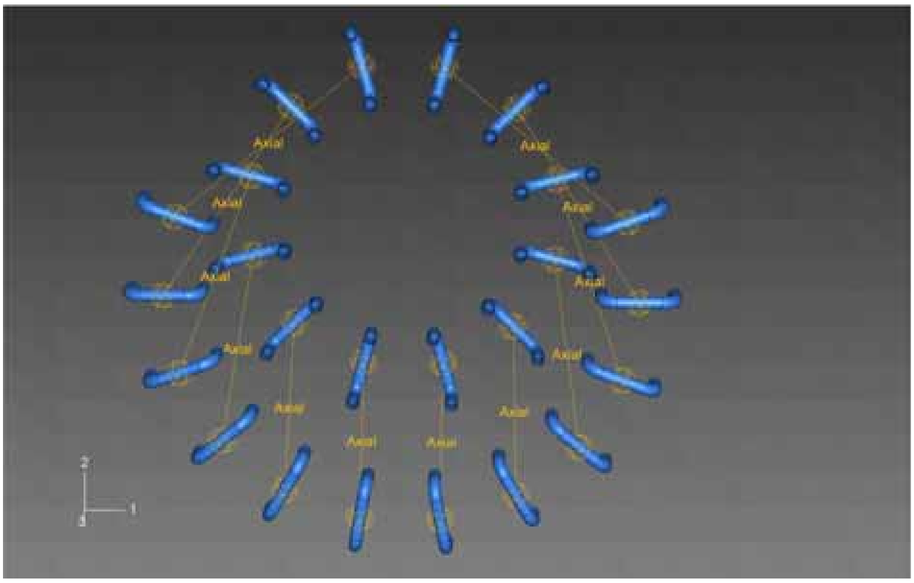

Figure 7.8: Axial Connectors used to model Interrupted Stitches

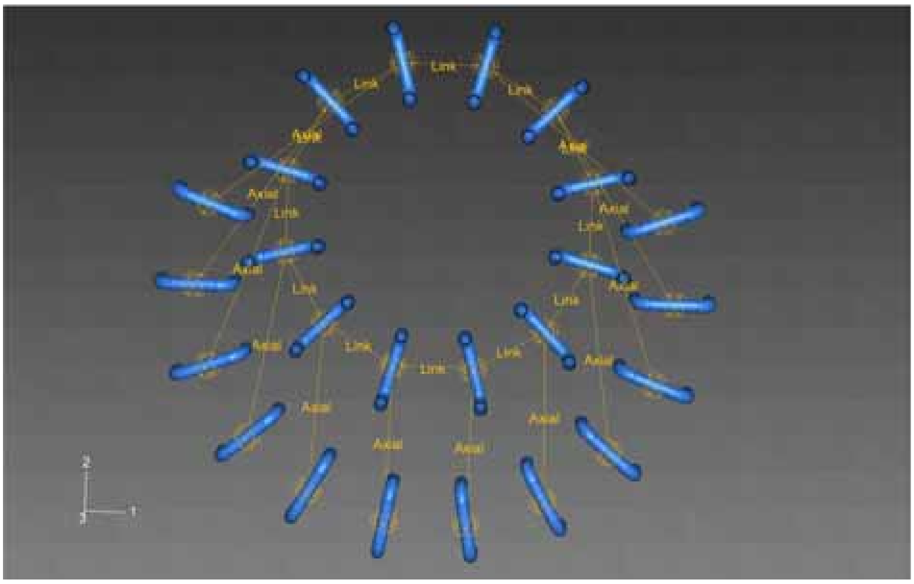

Figure 7.9: Link and Axial Connectors used to model Continuous Stitches

7.7 Load

The pressure loading *in vivo* is highly pulsatile. This was modelled in preliminary work (see Appendix B), but owing to the quasi-static assumption, the pressure was ramped from zero to the maximum pressure in the pulse profile.

In vivo, there is pressure on both the inside and outside of arteries and veins. The internal pressure is from the circulating blood, while the external pressure is from the tissue surrounding the arteries and veins. The pressure from the surrounding tissues was modelled as being constant throughout the systolic and diastolic phases. The value used was 14kPa, on the upper bound of the physiological range.

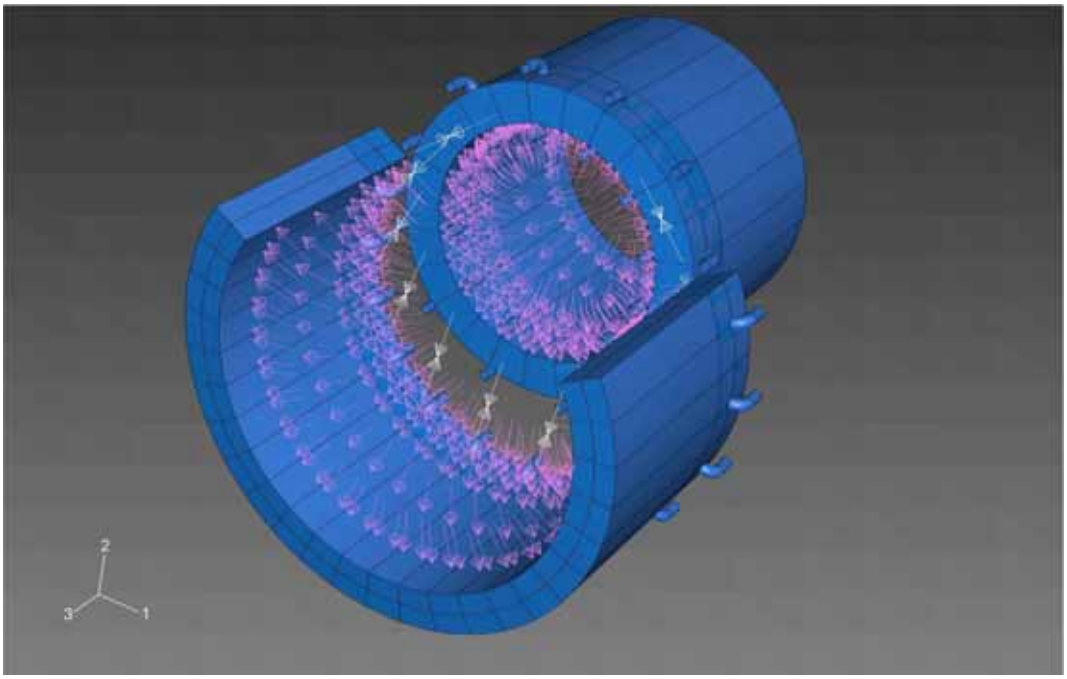

Figure 7.10: Connector Forces and Physiological Pressures

To close the sector, boundary conditions were implemented to move the four straight edges of the sector into their closed positions. See figure 4.3 for the bending process.

Once the sector had been closed, the inner surface was under compression, while the outer surface was in tension. Holzapfel *et al* [2] provides a reminder that the pre-stresses that are established in arteries result from various growth mechanisms of the different layers, making the stress situation more complex than considered here.

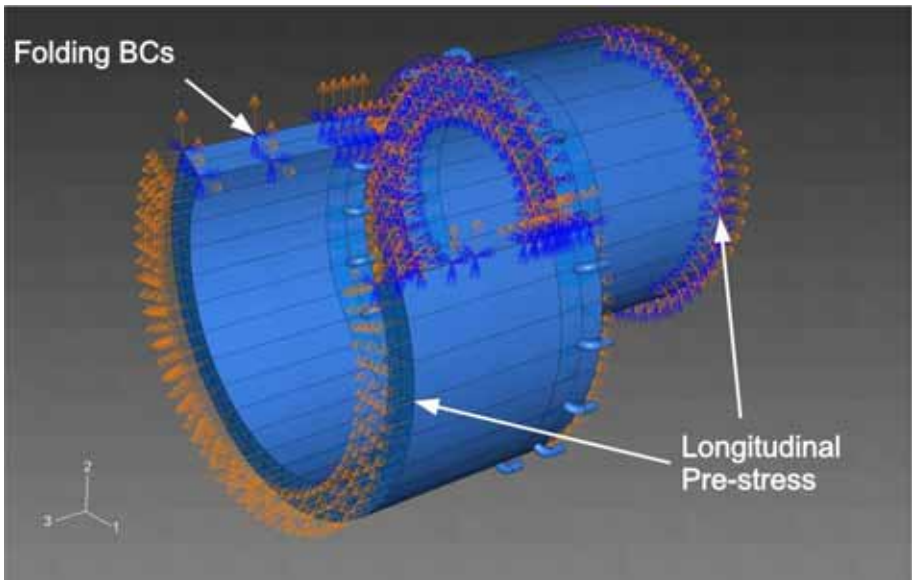

Figure 7.11: Boundary Conditions

Displacement boundary conditions were also used to create the initial longitudinal pre-stress. The end faces were each moved in opposite directions by 10% of the length of the section. This took place at the same time as the closing of the sector.

7.8 Mesh

Continuum elements were selected for all final analyses. The C3D8H element was selected. This is an eight-noded hybrid brick-element. Hybrid elements are intended primarily for use with incompressible and almost incompressible material behaviour, being compulsory for incompressible behaviour [9]. They are therefore appropriate for the material models employed.

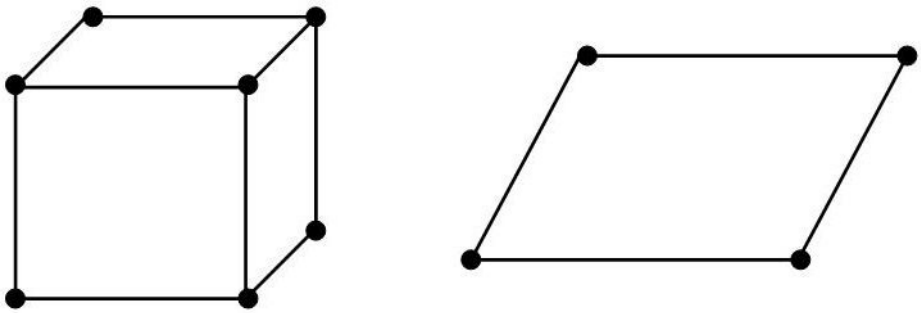

Figure 7.12: C3D8H Element on the left, R3D4 Element on the right

For many of the preliminary jobs, it was impractical to use hexahedral (hex) elements, due to the geometry. However, hex elements were used whenever possible, by extensively partitioning cells.

As mentioned, the parts were extensively partitioned to enable the use of hex elements. A further reason was to control the refinement of the mesh. The edges on the end of the section to be joined were individually seeded to control the shape of the mesh. The edges created by the longitudinal partitions were also individually seeded.

To mesh the "stitches", 4-node 3-Dimensional bilinear rigid quadrilateral elements (R3D4) were used. The "stitches" were modelled as discrete rigid shells in 3 dimensions, making only two elements available - R3D4 and R3D3. R3D3 elements are triangular facets. The meshing of the part constrained the size of the radii on the stitches, as elements on the inside of the radii became prohibitively small as the radii were decreased.

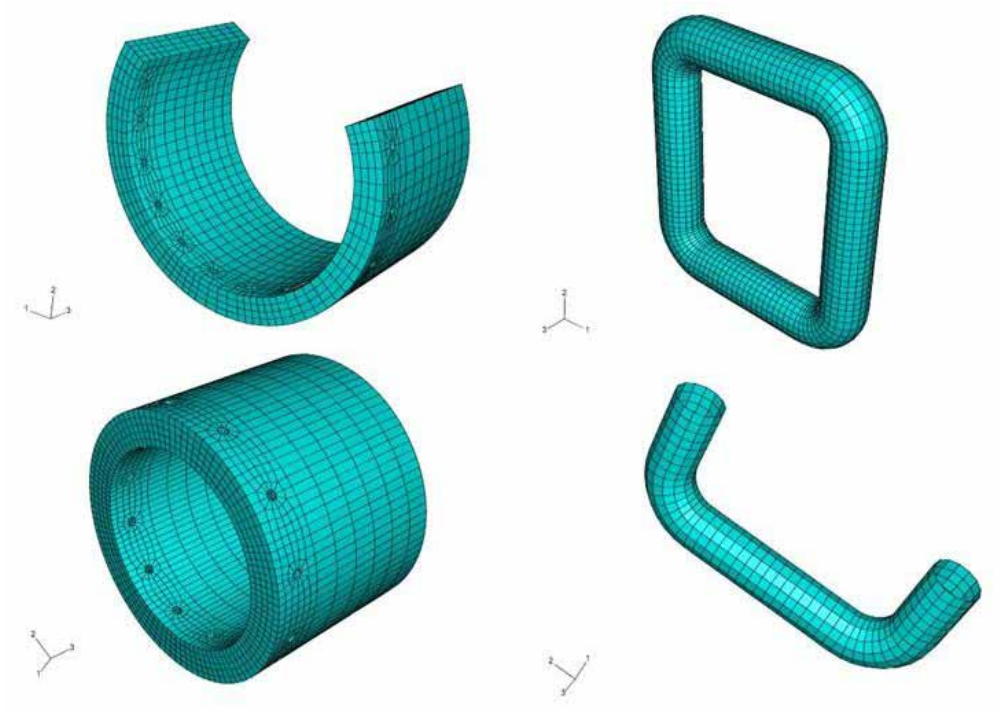

Figure 7.13: Components' Meshes
Number of elements clockwise from top left: Vascular 2848, UShape 658, Hoop 1372, Cyl7100

Chapter 8

Results

8.1 Introduction

The results presented below have been divided into 6 sections - a section for each configuration that was investigated. In $ABAQUS^{®}$ analyses, the units to be used are not specified. Instead, it is the user's responsibility to ensure that the values used are consistent. For example, if displacements are specified in meters(m) and forces in newtons(N), the pressure outputs from $ABAQUS^{®}$ will be in pascals(Pa). Note that in all of the models, the geometry was scaled up, as $ABAQUS^{®}$ was unable to display the 0.14mm diameter holes when meters were used (0.00014m). All geometrical features were therefore defined in millimeters, so the results have been scaled.
When viewing the results presented below, it is very important that they are considered in context. The implications of the conclusions and recommendations from chapter 9, "Verification of Results" must be kept in mind.
Some of the simulations were performed to establish a basis for comparison. These are presented below along with the more realistic results. All stresses are Maximum Principal Stress. All images are shown at scale 1:1.

8.2 Compliance Mismatch

It has already been stressed that a compliance mismatch between joined sections is problematic. As a simple preliminary demonstration of this, a single

cylinder was created and divided into two. Note that the geometry is symmetrical. Each portion was assigned a different set of material properties. To simulate the use of vascular sections from different parts of the body, the constants defining the vascular tissue were adjusted, as explained in Appendix A.

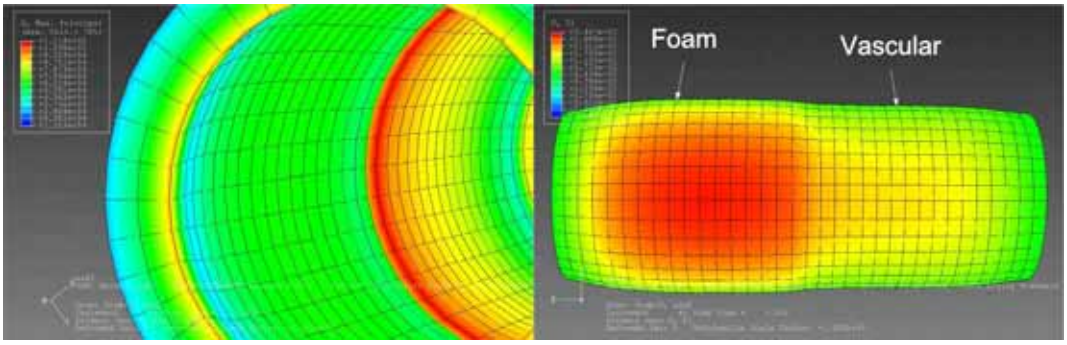

Figure 8.1: Foam and Vascular Sections
Max Stress(left): 0.11MPa, Max Radial Displacement(right): 0.35mm.
Note that the maximum stress is found on the first row of elements of the more compliant foam.

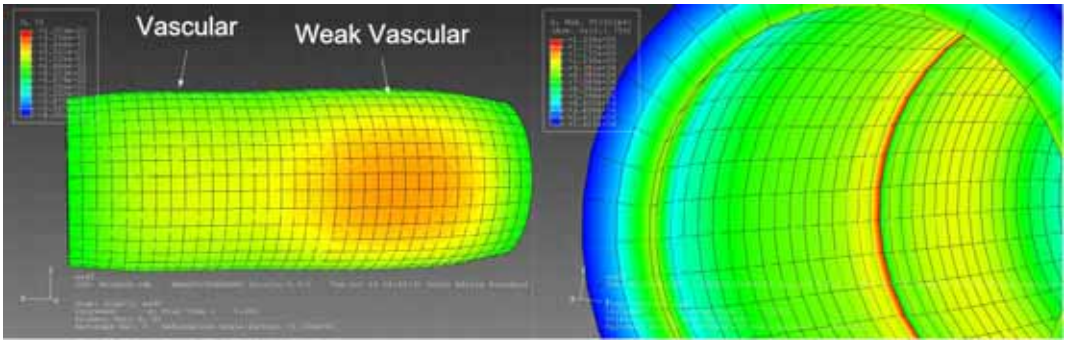

Figure 8.2: Vascular and Weakened Vascular Sections
Max Radial Displacement(left): 0.40mm, Max Stress(right): 0.13MPa.
Note again the location of the maximum stress.

When a simple vascular section is put into tension, the max stress is 0.1 MPa and the max displacement is 0.67mm.

8.3 Vascular to Vascular

The pre-stressing procedure is very similar between all of the vascular tissues modelled. The procedure is shown in figure 4.3.

8.3.1 Control Simulations

As a control, identical vascular sections were used to form an anastomosis. The results are presented below for comparative purposes.

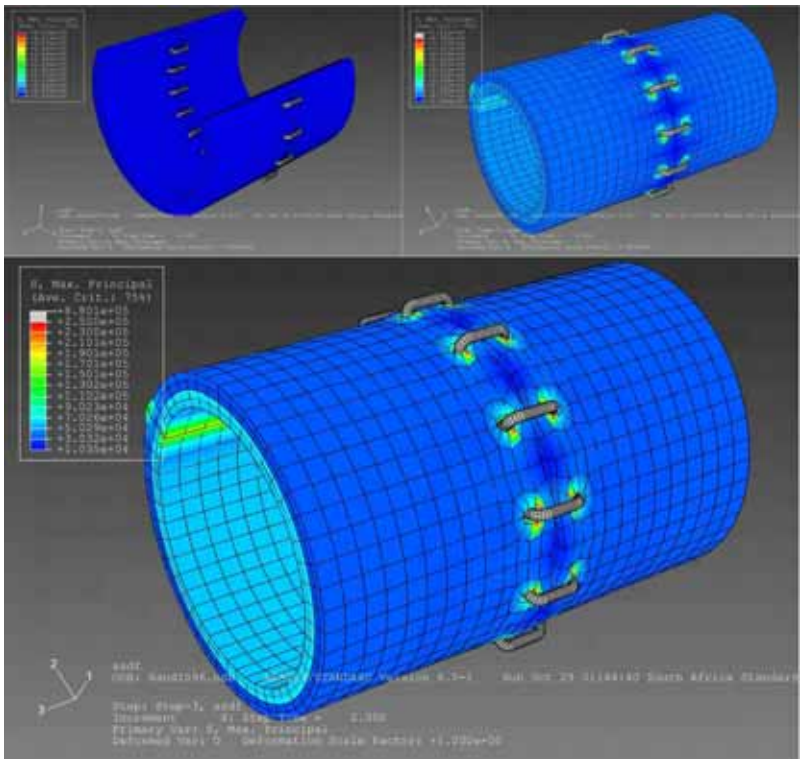

Figure 8.3: Vascular to Vascular, Interrupted
Top left shows initial configuration, top right shows configuration after pre-stressing and bottom shows max pressure. Stress Range Plotted: 0.01MPa to 0.88MPa.

8.3.2 Realistic Simulations

Instead of using the same vascular material to model both sections, each vascular section is assigned its own properties for both the media and adventitia.

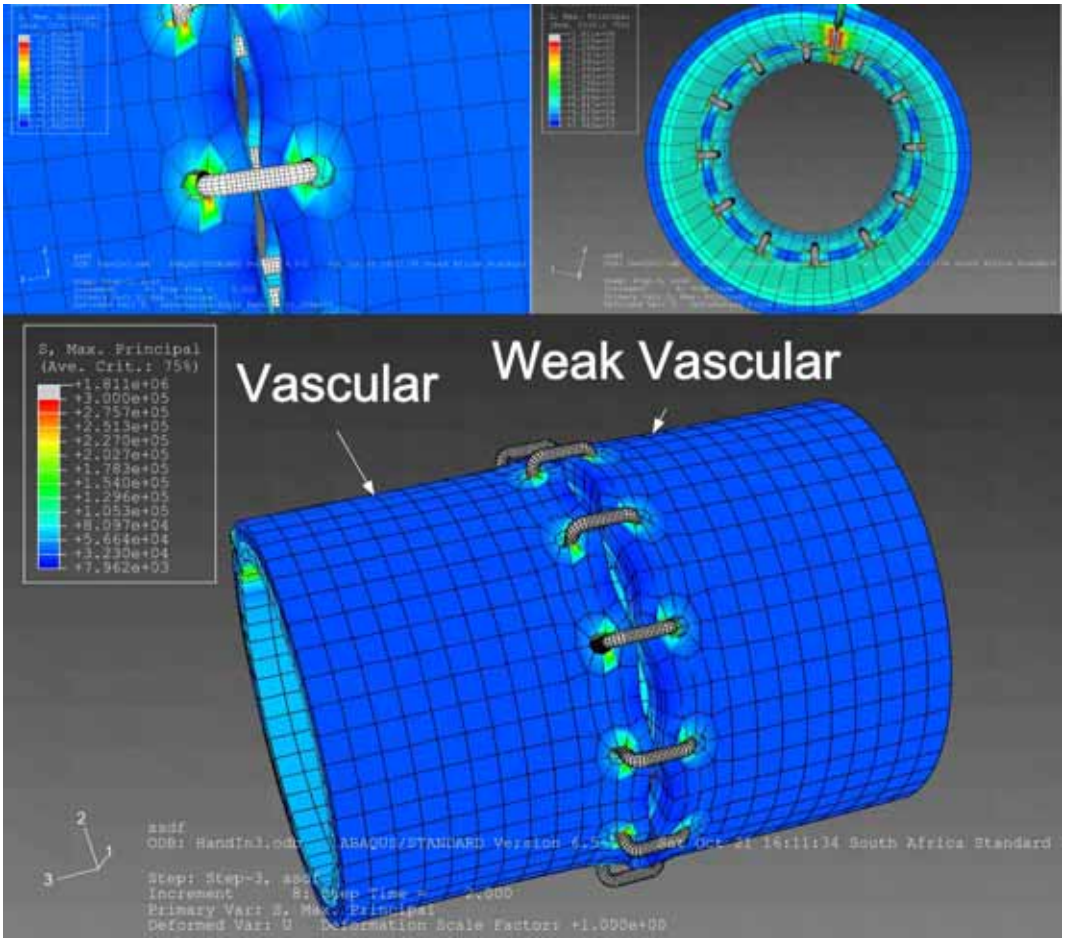

Figure 8.4: Vascular to Weak Vascular, Interrupted
Note the bowing between the stitches. Stress Range Plotted: 7.90kPa to 1.80MPa.

Notice the pronounced "bowing" between the stitches. It would be useful to study this phenomenon with a fluid mechanics program, in order to make recommendations on the number of stitches to create. Some superficial mechanical investigations concerning this problem were run. See Appendix C.

Notice the large difference in the outer diameters of the weakened vascular and vascular tissue. On the following page, the illusion is given that the interrupted anastomosis (top) has a smaller dilated internal diameter than the continuous anastomosis. This is because the far section of the interrupted anasomosis has not "flared" like its continuous counterpart.

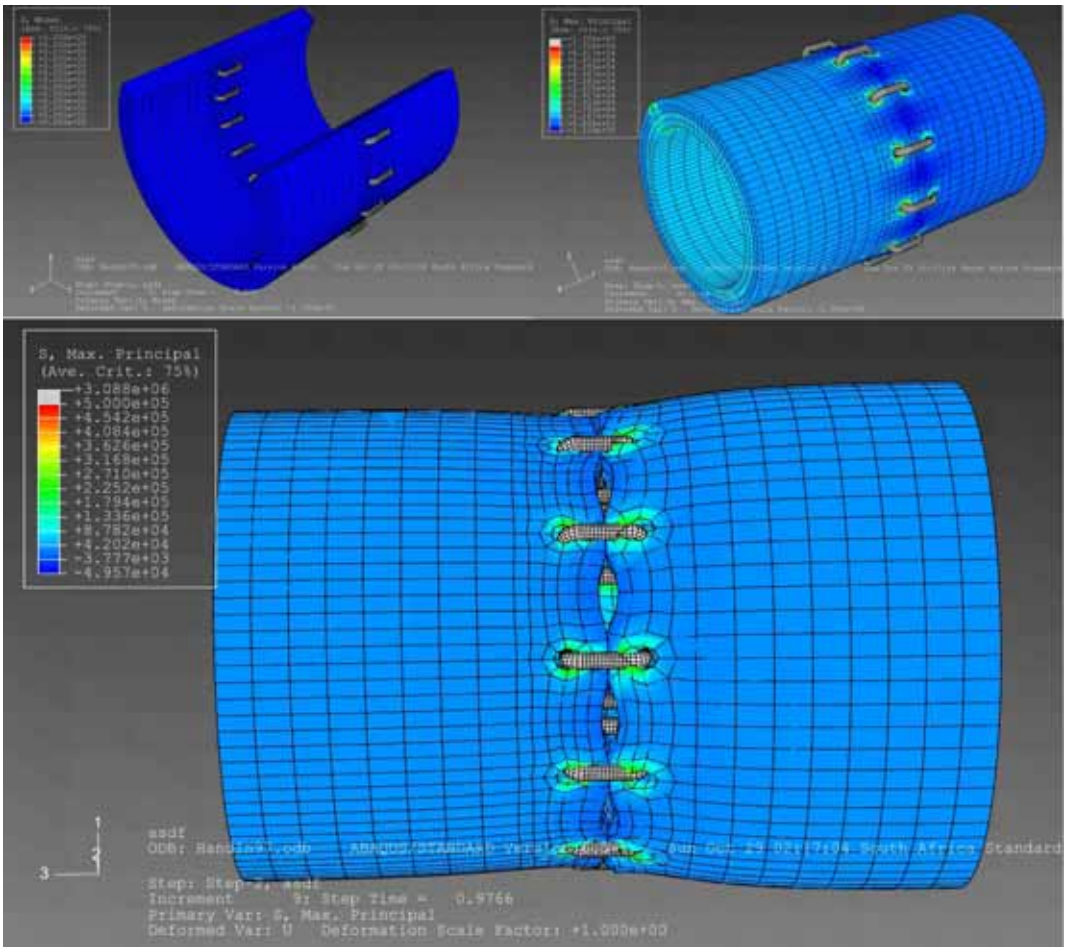

Figure 8.5: Vascular to Weak Vascular, Continuous
From top left: Initial configuration, circumferentially and axially pre-stressed, max pressure. Stress Range Plotted: 0.05MPa to 3.08MPa.

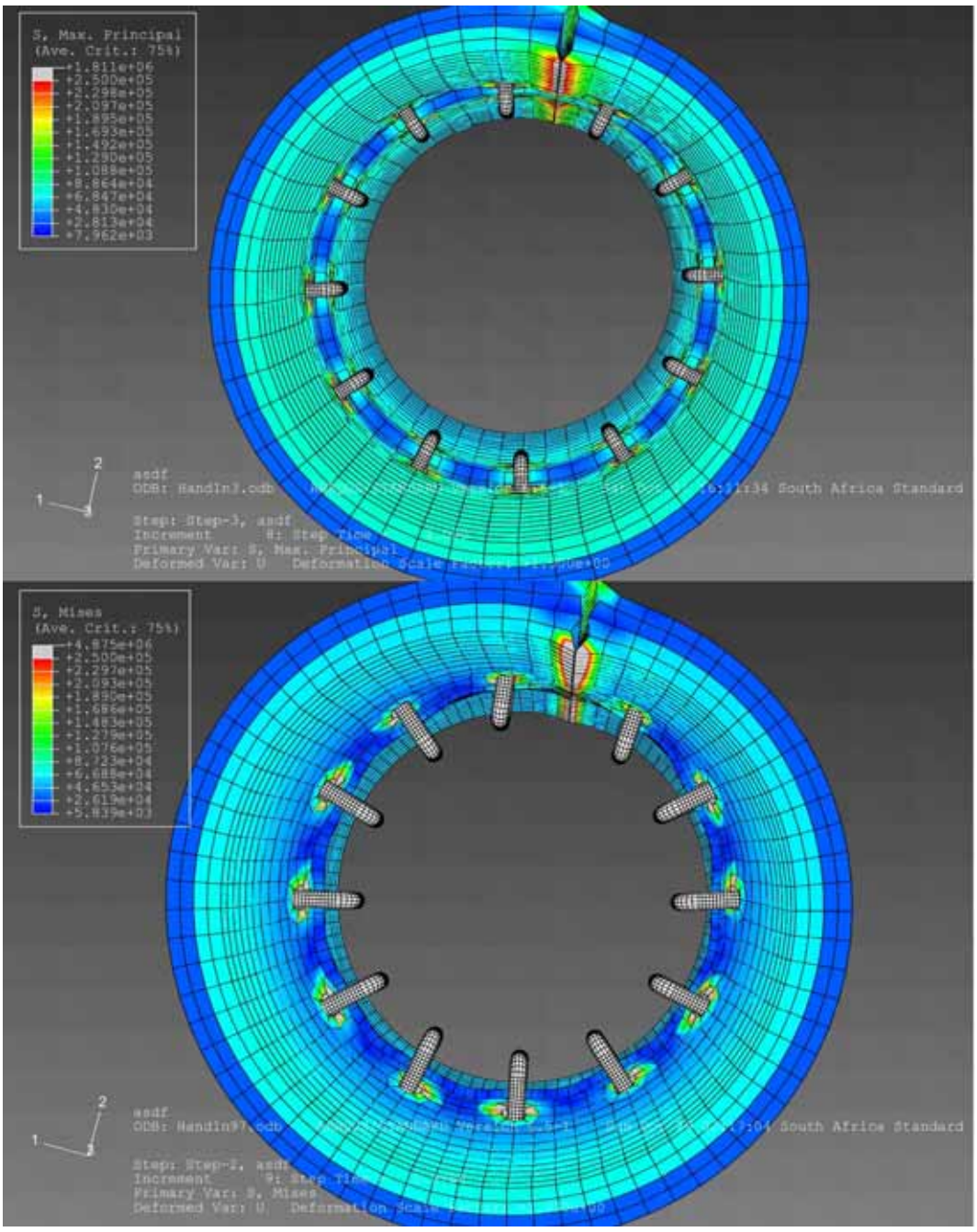

Figure 8.6: Vascular to Weak Vascular, Continuous and Interrupted View down the axis of the anastomoses. Only stresses less than 0.25MPa are coloured, in both cases. The scale is identical in both.

8.4 Vascular to Synthetic

The synthetic material is also pre-stressed longitudinally, to the same extent as the vascular tissue, to model the in vivo conditions. The synthetic sections are not circumferentially pre-stressed, as the manufacturing processes does not warrant it. No control simulations were done for this configuration.

8.4.1 Realistic Simulations

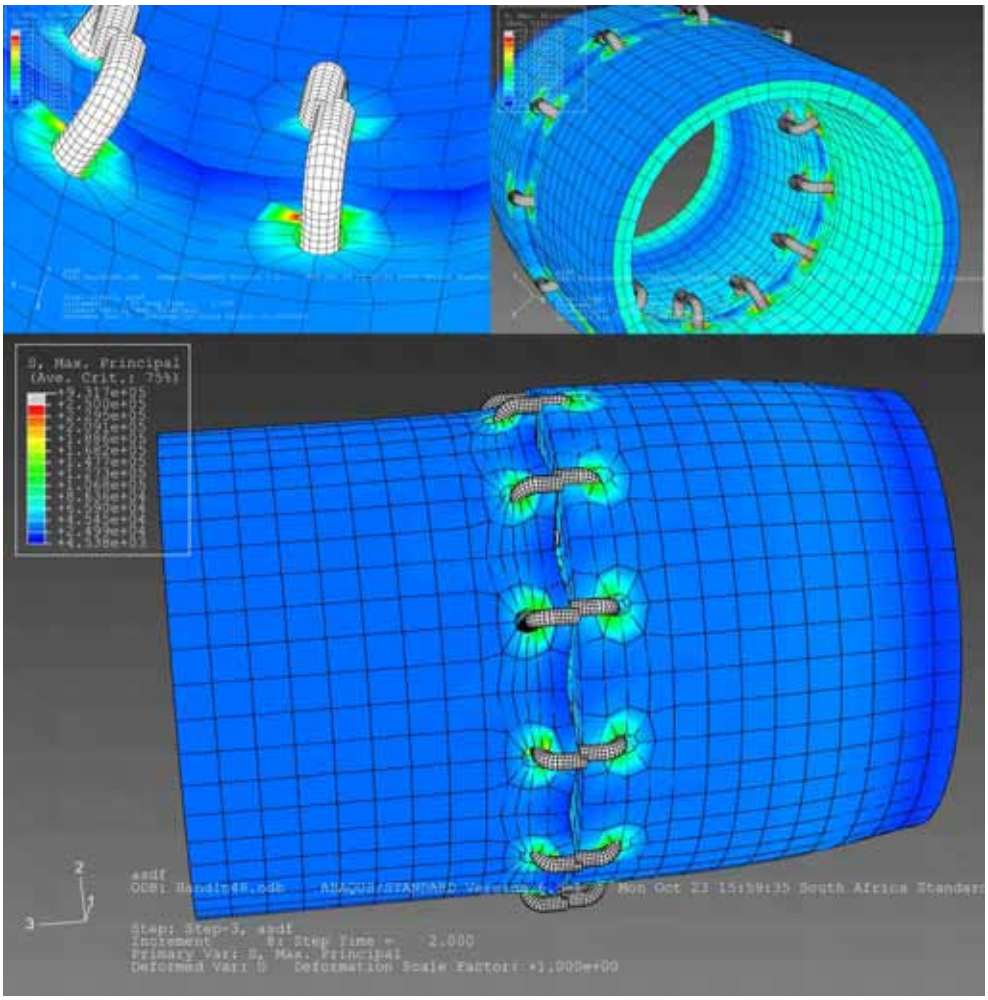

Figure 8.7: Vascular to Synthetic, Interrupted
The stitches (top left) don't aligned perfectly, as reference points at their centres of mass are connected. Stress Range Plotted: 4.54kPa to 0.90MPa.

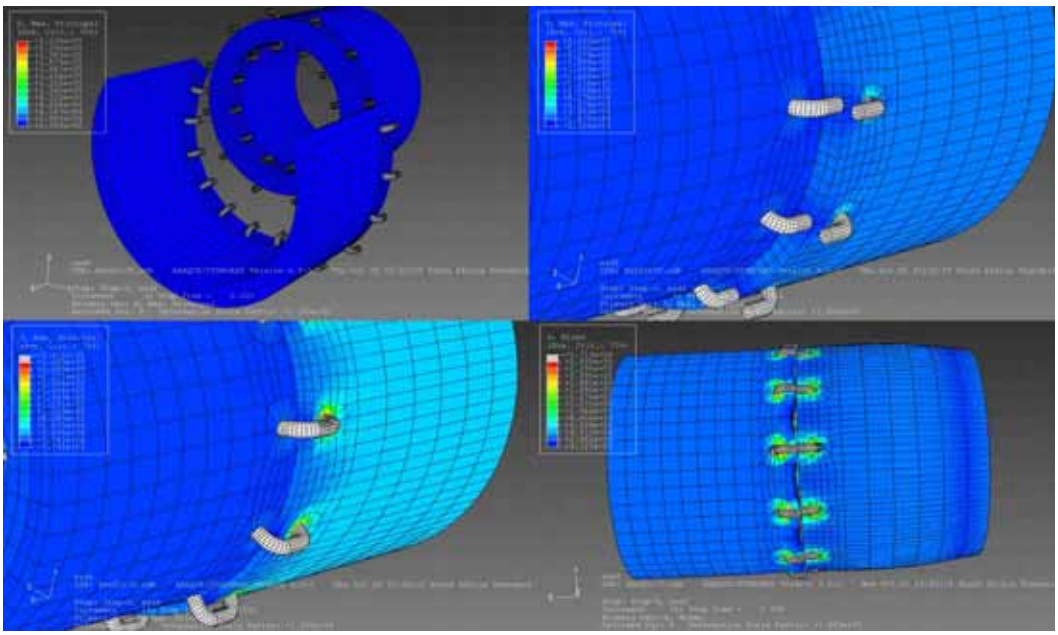

Figure 8.8: Vascular to Synthetic, Continuous
The process by which the stitches align is shown above. After the pre-stressing, the U-shaped stitches don't align (top right). This is corrected by applying a contracting force on the axial connectors (bottom left). Stress Range Plotted: 4.12kPa to 1.70MPa.

8.5 Synthetic to Synthetic

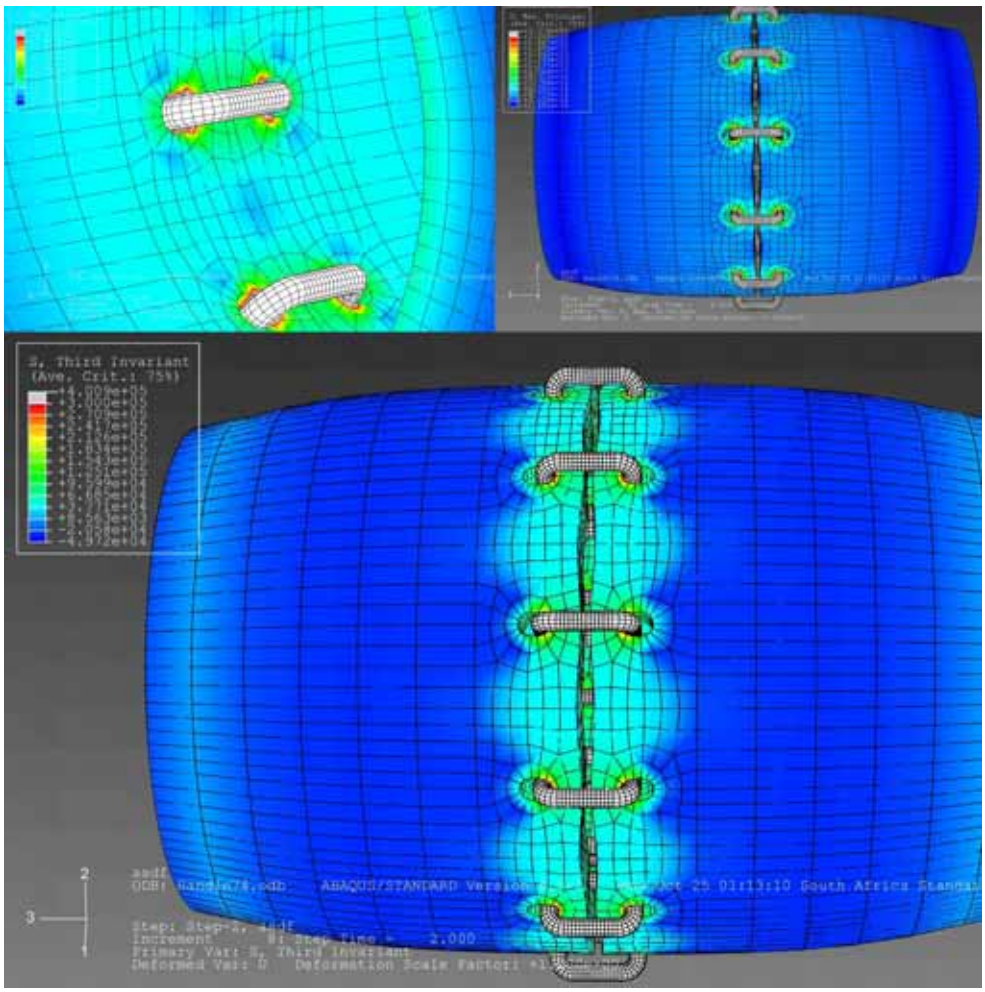

Figure 8.9: Synthetic to Synthetic, Interrupted
The maximum principal stress is plotted in both of the top two images. In the lower image, the stress with respect to the third invariant is plotted. This stress is given by $det(\sigma) = \sigma_1\sigma_2\sigma_3$. It is used because of the way it illustrates the stress concentrations around the stitches. Stress Range Plotted: 0.02MPa to 0.34MPa.

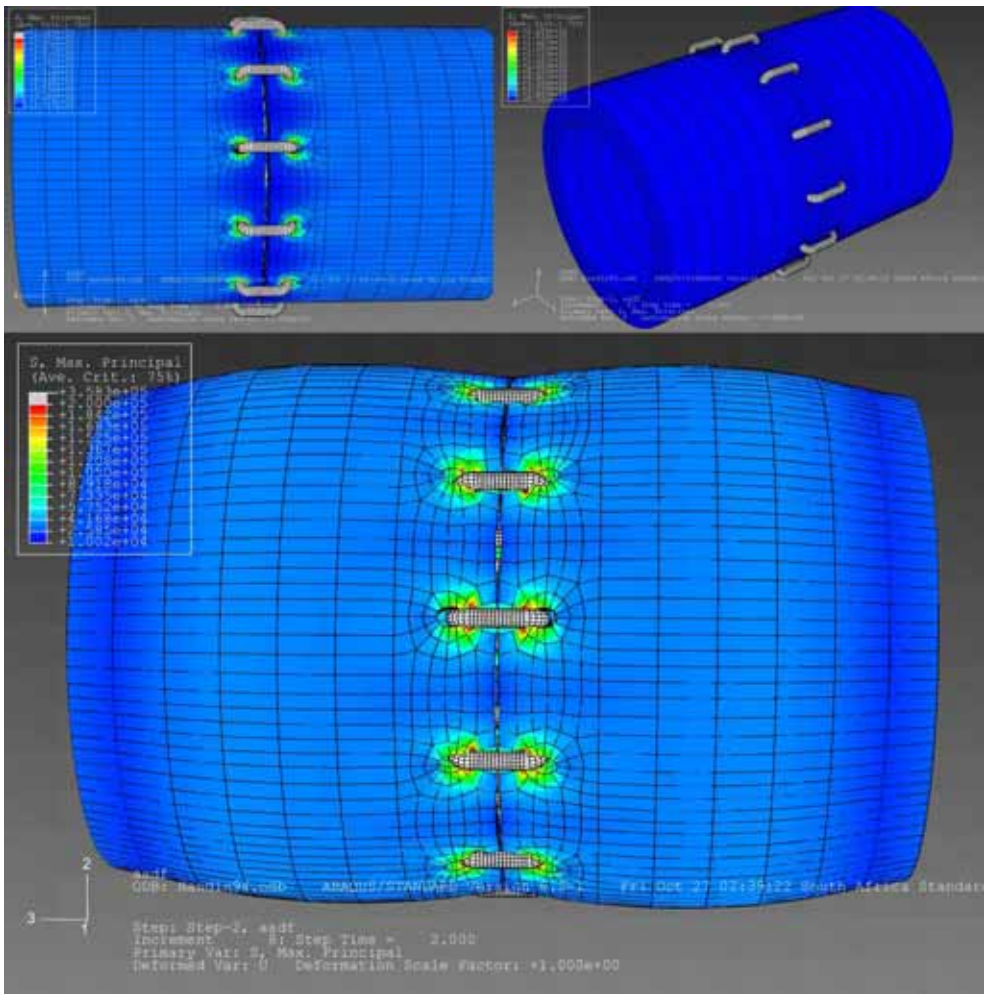

Figure 8.10: Synthetic to Synthetic, Continuous Stress Range Plotted: 0.01MPa to 0.36MPa.

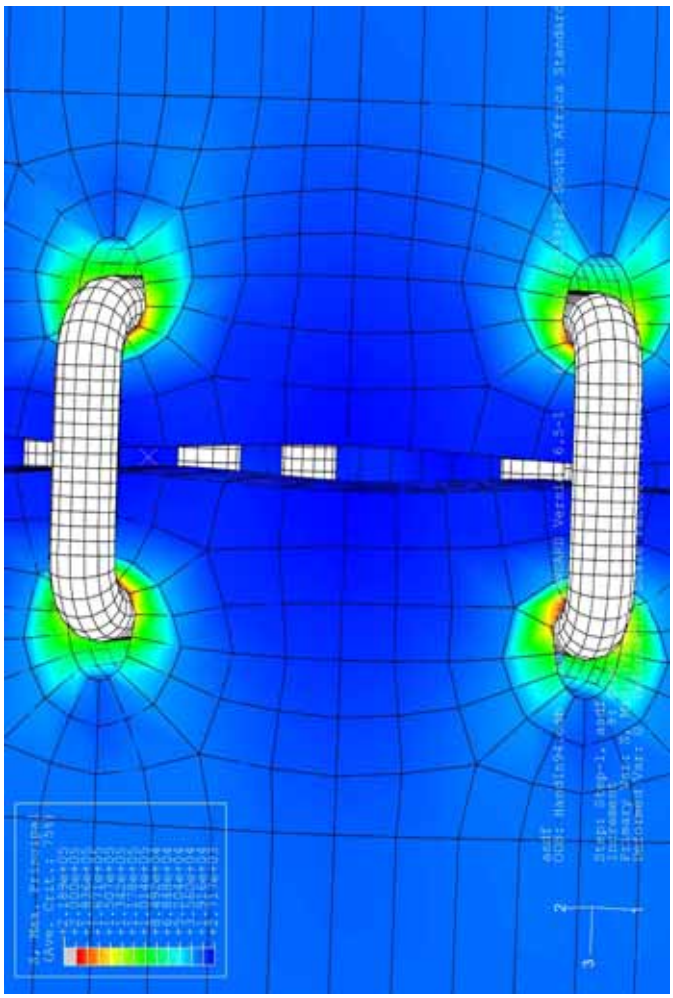

Figure 8.11: Synthetic to Synthetic, Continuous
This image illustrates the maximum principal stress concentrations that surround the stitches. The deformation of the holes as well as the "bowing" between the stitches is particularly clear in this simulation.

8.6 Comparisons

In all of the images shown below, the maximum stress that was coloured was 0.25MPa and the minimum stress that was coloured was 0.03MPa. The same scale is used on all of the images. The large grey areas represent stresses that are lower than 0.03MPa, while the small grey areas around the stitches are areas where the stress is greater than 0.25MPa. These figures show that although the maximum stress varies considerably between the various configurations, it is often the result of a single very high stress concentration. The stresses are generally comparable. The maximum stress in each figure is given.

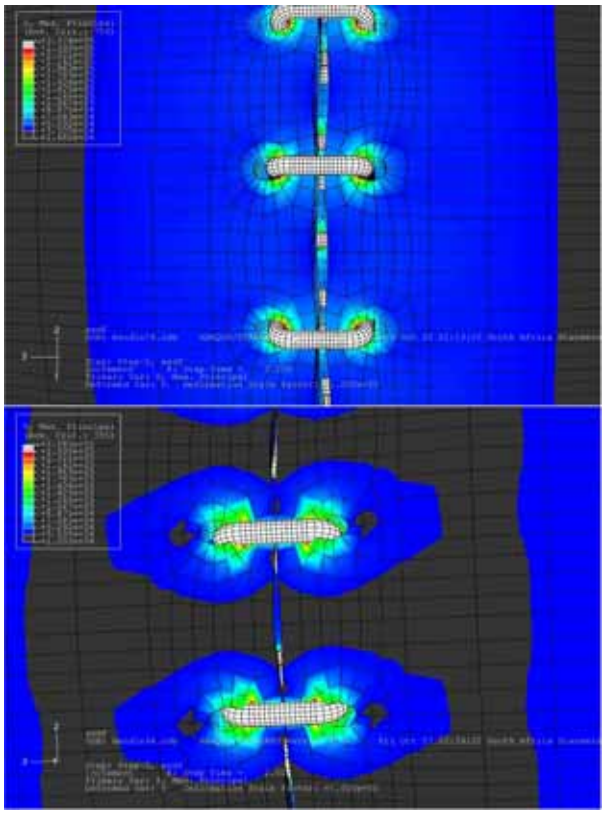

Figure 8.12: Synthetic to Synthetic with Limited Scale
Interrupted on top, continuous beneath. Max stress: 0.36MPa

A further observation is the different distribution patterns obtained from continuous and interrupted stitching. While the interrupted technique seems to produce smaller areas of low stress, it is noticeable that it also produces lower maximum stresses. Continuous stitching produces larger low-stress areas and smaller high-stress areas, but the maximum stresses are higher than those from interrupted stitching. Continuous stitching produces significant stress gradients. The following images illustrate these points (the image on the next page in particular).

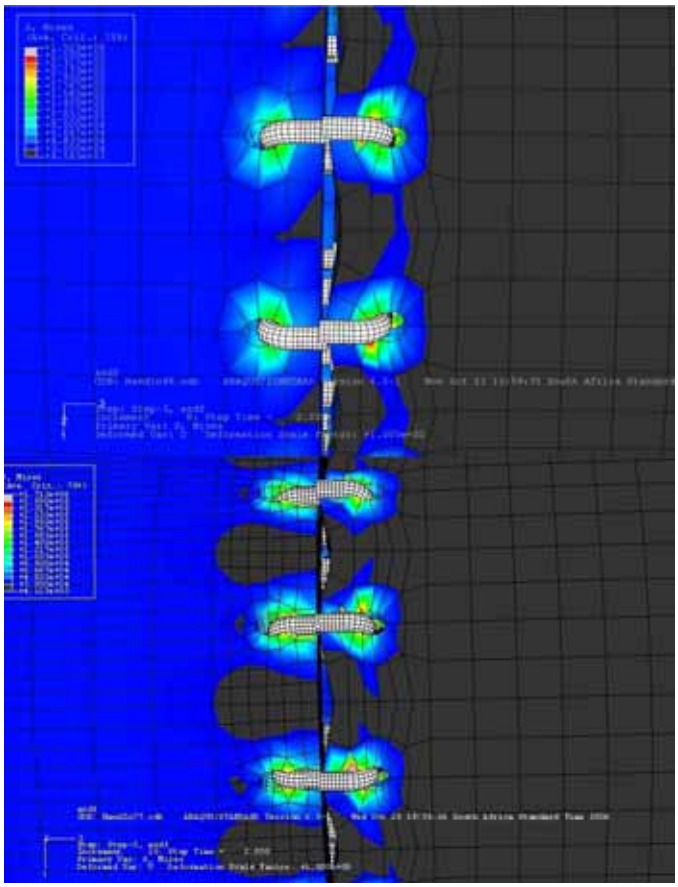

Figure 8.13: Vascular to Synthetic with Limited Scale
Interrupted on top, continuous beneath. Max stress: 1.71MPa

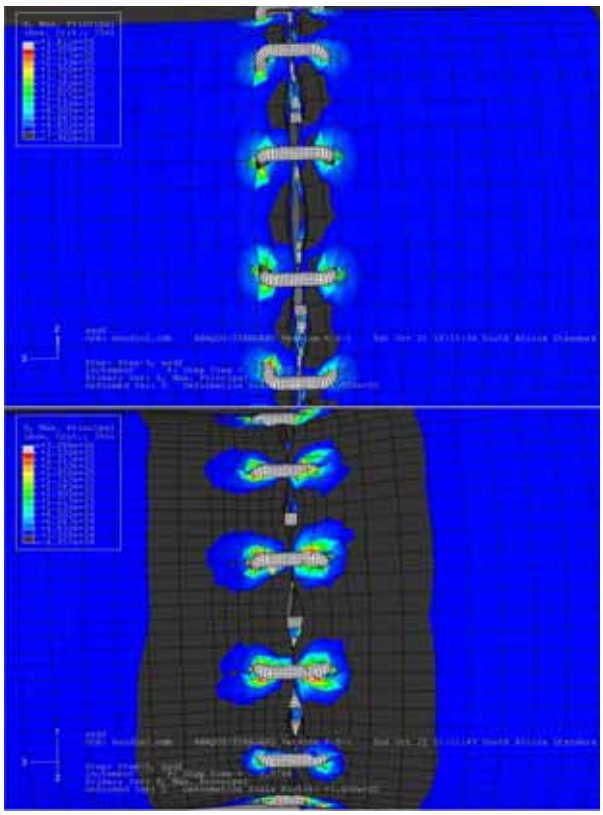

Figure 8.14: Vascular to Vascular with Limited Scale
Interrupted on top, continuous beneath. Max stress: 3.09MPa

By comparing the maximum stresses only (0.36, 1.71 and 3.09MPa), it would seem as if the analyses are substantially different. However, when the peak and minimum stresses are removed, the results become remarkably similar. When considering the different mesh structures employed in the simulations, and referring to chapter 9 "Verification of Results", the contour maps presented below bear a great deal more weight. The final observation then, is that the continuous stitches stress less of the graft than the interrupted stitches, but the areas which are stressed, are stressed more heavily.

8.7 Diameter Matching

The negative effects of a compliance mismatch can be minimized by matching the diameters of the respective sections correctly. It is important to match the diameters of the sections under physiological conditions (pressurized). The images below illustrate an attempt made to match the diameter of the foam section with that of the vascular.

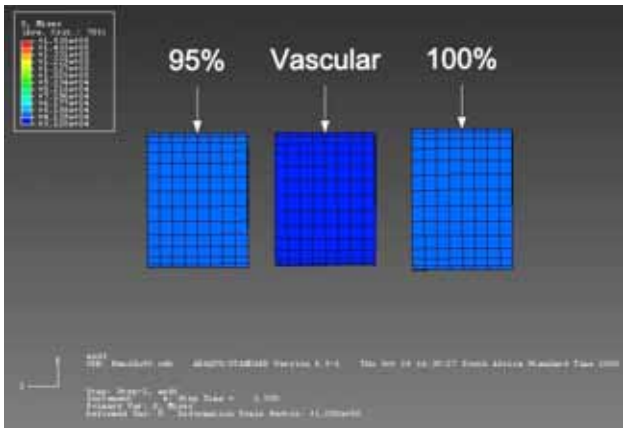

Figure 8.15: Size Matching at Physiological Pressure
Stress Range Plotted: 0.01 to 0.88MPa.

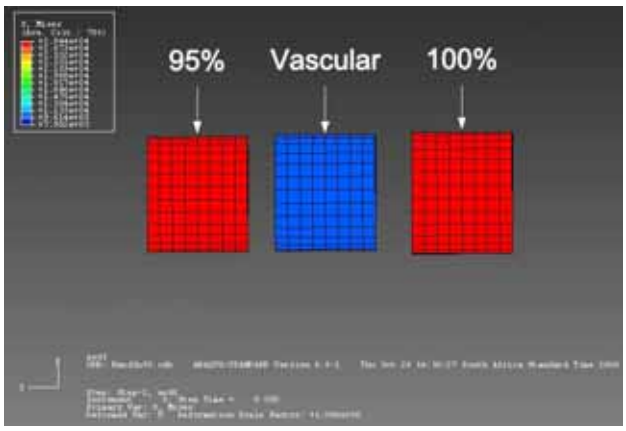

Figure 8.16: Size Matching at Atmospheric Pressure (Pre-stressed)
Stress Range Plotted: 0.01 to 0.88MPa.

8.8 Summary

The relevance and accuracy of the results is discussed further in chapter 9, "Verification of Results". The following table summarises the maximum principal stresses that were encountered in each simulation. Based on the results below, qualatative as they may be, the interrupted technique yielded lower stresses in all of the simulations, sometimes by as much as a factor of two. Which pattern to select and implement is not a trivial decision and is discussed in 10.1, "Stitching Pattern".

	Interrupted	Continuous
Vascular to Weak Vascular	1.80	3.08
Vascular to Synthetic	0.90	1.7
Synthetic to Synthetic	0.34	0.36

Table 8.1: Summary of Results (MPa)

Chapter 9

Verification

9.1 Introduction

All finite element simulations, by definition, discretise the problem at hand. By creating a finite mesh on a part, certain assumptions are made and accuracy is lost. Whether a circle may be approximated with 4, 6, 12, 24 or 48 straight lines depends on the convergence of the mesh. Mesh is said to be converged when refining it produces negligible changes in the solution. What exactly "negligible" is, depends heavily on the problem at hand.

9.2 Increasing Computational Cost

The *ABAQUS*® user manual [9] states that calculating computational cost is not a straight-forward procedure. From their experience, they propose that computational cost is "roughly proportional" to the square of the number of degrees of freedom. The example that they use to explain this is a three-dimensional model with uniform, square elements (similar to those used in the full analyses in this work). They estimate that by refining the mesh by a factor of two in all three directions, the number of degrees of freedom increases by approximately 2^3, leading to a computational cost increase of about $(2^3)^2 = 64$. According to the manual, the disk space and memory requirements increase in the same manner, although it states that the actual increase is difficult to predict.

9.3 Methodology

In an attempt to verify the stresses and displacements indicated by the various models, a representative portion ($\frac{1}{12}^{th}$) of one of the investigated double-layered vascular sections was meshed with different densities. Loads and boundary conditions similar to those in the full analyses were applied to the sample. The elements that were used were the same as those used in the full analyses (C3D8H), with the same partitioning structure. The seeding pattern is slightly different, as attempts to refine the mesh around key areas were made in the full analyses. The only difference between the jobs illustrated below is their mesh densities.

In order to establish whether the displacements converged, a point (the same on each mesh) undergoing large radial displacement was investigated. The results are given in table 9.1 below.

Table 9.1 illustrates the parameters and results of the investigation. The stress after the initial axial pre-stressing is given, along with the stress after pressurising. The CPU time for each job is given along with the "Total" time, the time for the entire analyses. Note that the Max Principal Stess is given in table 9.1.

	Coarse	Medium	Fine
Elements	304	1980	11050
Stress in Tension (MPa)	0.085	0.168	0.275
Stress after Pressure (MPa)	1.701	1.762	4.241
CPU Time (s)	22	148	2258
Total Time (s)	52	240	10703
Radial Displacement (mm)	0.526	0.545	0.570

Table 9.1: Verification Parameters and Results

9.4 Meshes and Results

The meshes and Max Principal Stresses that are shown below are the actual plots from the analyses.

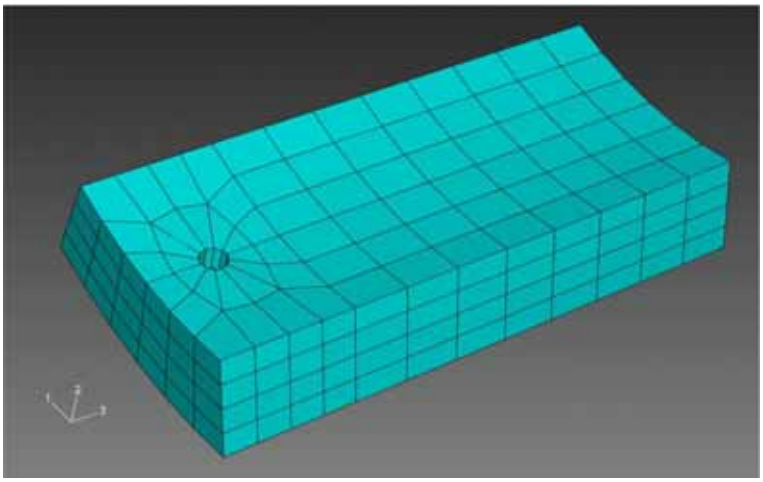

Figure 9.1: Coarse Mesh

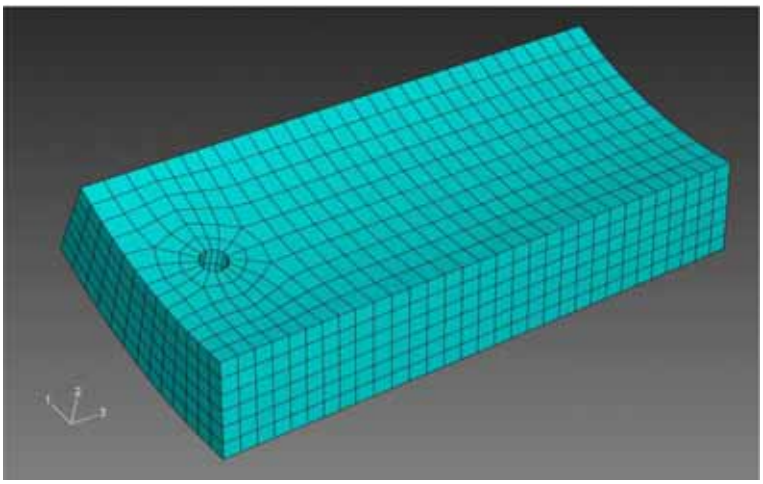

Figure 9.2: Medium Mesh

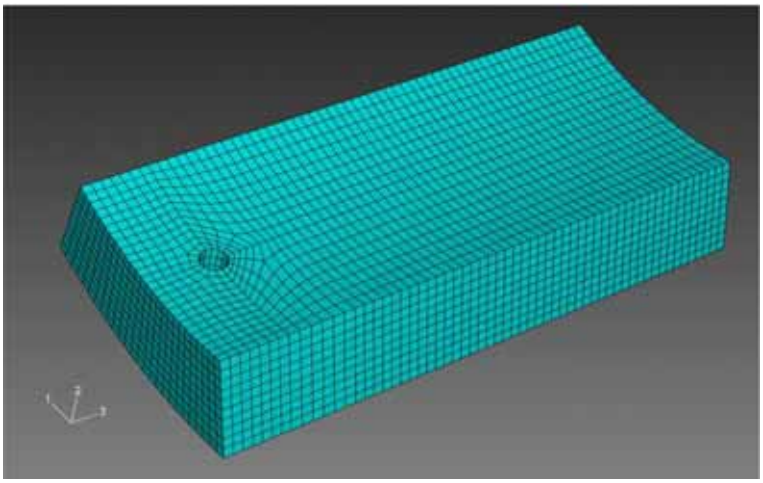

Figure 9.3: Fine Mesh

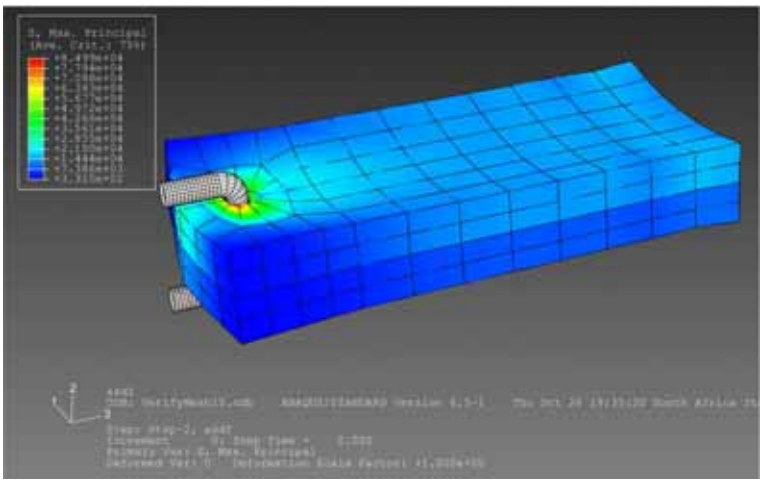

Figure 9.4: Coarse Mesh, Tensioned

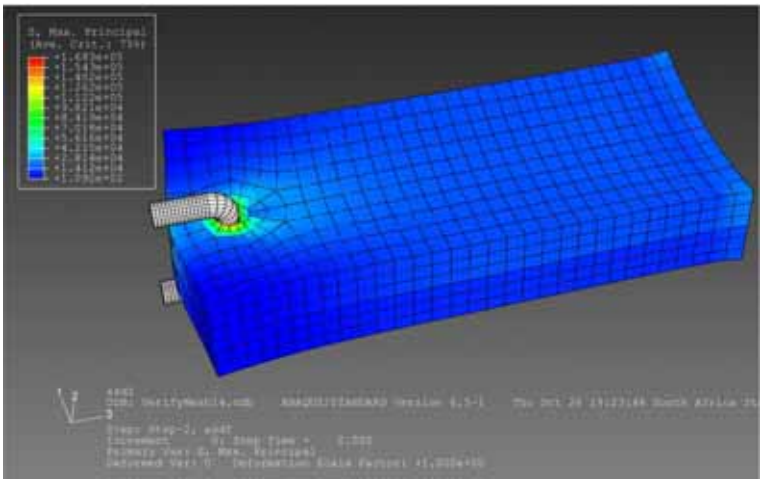

Figure 9.5: Medium Mesh, Tensioned

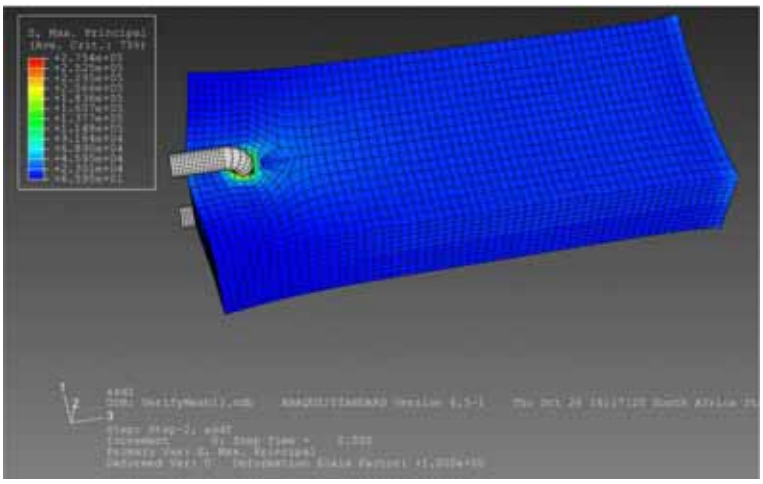

Figure 9.6: Fine Mesh, Tensioned

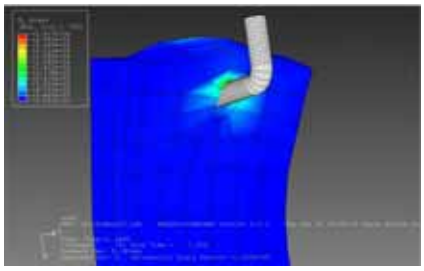

Figure 9.7: Coarse Mesh, Tensioned and Pressurised

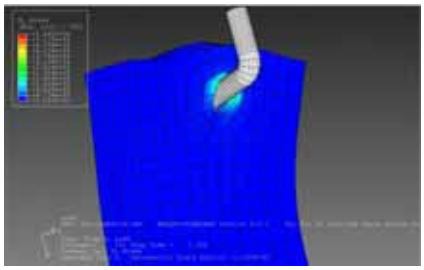

Figure 9.8: Medium Mesh, Tensioned and Pressurised

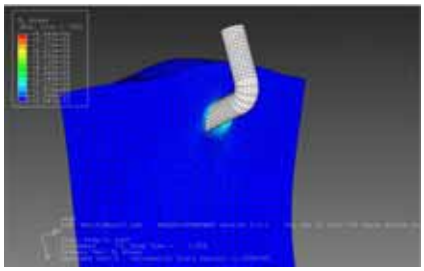

Figure 9.9: Fine Mesh, Tensioned and Pressurised

9.5 Conclusion

As can be seen from the results above, the fine mesh gives quantative results that vary considerably from those of the coarse and medium meshes under full load. However, at half-load, the following Mises stresses were obtained. The results suggest that the medium mesh is converging toward the fine mesh at lower stress. However, at high stresses and strains, the difference is significant.

	Coarse	Medium	Fine
Stress at Half Pressure (MPa)	1.189	2.453	2.883

Table 9.2: Mises Stress at Half Pressure

For this reason, it is advisable for the numerical results obtained to be viewed with a critical eye. That said, the deformations agree very well (within 10% of each other, table 9.1) and may be viewed as having converged.
As a final consideration, following the reasoning of the *ABAQUS*® user manual [9] and assuming no mesh refinement, a full analysis with a fine mesh would take almost 4 days of computational time. The total time would easily exceed a week. However, as explained above under "Increasing Computational Cost", increasing computational time is not the only limiting factor. The memory required to run a full job with a fine mesh would be very large and given that the machine used for these analyses had 512MB of RAM, the necessary use of large amounts of virtual memory would elongate the computation still further. Due to these limitations, most of the final simulations that were run utilised either the medium or the coarse mesh.

Chapter 10

Conclusions and Recommendations

10.1 Stitching Pattern

In all of the analyses run, the interrupted technique outperformed the continuous technique with respect to stress concentration an magnitude. However, a recommendation to always use the interrupted technique does not automatically follow from the results. Once in place, it is clear that the interrupted technique is superior, but that is only looking at the advantage of the interrupted pattern. In the same way, looking at the performance of the continuous pattern only once it is in place is to only look at the disadvantage of the technique. In order to make a definitive recommendation, it would be necessary to gauge the extent to which handling affects the well-being of the vascular tissue. That said, even though the effect of physical handling has not been quantified, the interrupted technique is so far superior with respect to compliance and stress concentration, that it is tempting to recommend it. It is possible to make several suggestions to reduce the negative impacts of the interrupted technique, such as the adoption of the "no touch" technique mentioned by Lemson *et al* [1]. This is the case for the continuous method too. The method is flawed mainly in that the anasomosis so formed is excessively rigid. If it were possible to increase the compliance of the anastomosis by adopting a much more elastic suture material, the continuous

suture would have the advantages of the interrupted technique without the disadvantages.

10.2 Synthetic Material

The synthetic material that was developed at the CVRU by Yeoman [8] was used in this work. Although most synthetic materials in use (ePTFE, Dacron, Silicone) are considerably stiffer than the native artery, the hyperfoam material that was modelled is *more* compliant than the vascular tissue. The problem, as mentioned before, is not necessarily that the graft material is stiffer than the native, but rather that there is a compliance mismatch. The problem remains with this material. Research is currently being done on a wire mesh that may be used to envelop the hyperfoam, simulating the action of the adventitia.

Although a compliance mismatch exists between the native tissue and Yeoman's material, it is not conclusive that this material is unsuitable in its unmodified state. The justification behind this is based on the observation made by Tiwari *et al* [27] that ePTFE is reduced to 14% and Dacron to 29% of its preimplantation compliance after 3 months of implantation. It is therefore recommended that the suitability of Yeoman's material be investigated over an extended duration *in vivo*.

10.3 Material Model

A hyperviscoelastic material model, proposed by Saleeb *et al* [22] has been formulated to simulate complex biological tissues in $ABAQUS^{®}$. The model allows for the definition of helically arranged fibre reinforcements for individual elements, allowing the anisotropy of these tissues to be modelled. A further advantage of the model is its computational efficiency compared to the complex conventional methods of defining anisotropic fibre reinforcements.

With a view to implementing the model in this work, it was requested in mid September 2006, but was only received in mid October 2006. It unfortunately came with no instructions with respect to the system requirements nor

implementation and although prolonged attempts were made to reproduce the author's demonstrative tests, no usable results were obtained. Further assistance was requested the next day, but as of 31 October 2006, no response has been received.

It is believed that this model is highly suitable for the modelling of biological tissues and it appears to be very comprehensive. For these reasons, it is strongly recommended that the model is pursued further and implemented in future work. A licence for the model, expiring in October 2007 was obtained.

10.4 Dynamic Studies

Although there is a considerable amount to be gained from quasi-static analyses, the phenomenon that is being modelled is a dynamic one. It is unfortunately not possible to incorporate user-defined hyperelastic behaviour into $ABAQUS^{®}$\Explicit with a UHYPER, nor is it possible to use the material model proposed by Saleeb *et al.* Be that as it may, there may be a considerable amount to be learnt from a dynamic model incorporating simplified materials that may be modelled in Explicit.

10.5 Fluid-Solid Interaction Studies

The influence of fluid mechanics on the performance of grafts is arguably more important than that of the solid mechanics. Lemson *et al* [1] mentions that numerical simulation model studies of a distensible end-to-side anastomosis "confirmed the fact that compliance mismatch was not an important factor in the development of intimal hyperplasia." "It is suspected that the effects of wall distensibility are less pronounced than those brought about by changes in arterial geometry and flow conditions." Although it is commonly believed that both solid and fluid mechanics play significant roles in the formation of IH, the point is well taken.

It is desirable to model the *in vivo* conditions of anastomoses making as few assumptions as possible, as realistically as possible. In order to reproduce *in vivo* conditions, the intimately related fluid dynamics and solid mechanics

of arteries need to be modelled together so that their influences on each other and on anastomotic performance may be understood.

10.6 Clinical Studies

Although computational models are powerful tools, they have their limitations. It is extremely difficult to model biological tissue, due to complex growth patterns, irregular mechanical and geometrical properties, etc. Clinical methods have their limitations too, the most grave of which is the difficulty in measuring mechanical properties *in vivo*. That said, it is not possible to model certain aspects of anastomoses in any other way. The plethora of biological variables (pH, enzyme action, growth patterns, ionic concentrations, etc) make computational models seem hopelessly inadequate in providing accurate results. The numerical modelling of the graft stiffening mentioned in chapter 10.2, "Synthetic Material" would be extremely complex. Not only would clinical studies broaden understanding, but would also serve to verify and guide computational work.

10.7 Computational Power

As was described in "Verification of Results", substantial computational power is required to obtain accurate, quantative results. Therefore, if this sort of result is sought after, it is recommended that a highly refined mesh is run on a cluster.

Appendix A

Computer Codes and Implementations

A.1 Python code

ABAQUS® consists of a user-interface known as CAE. This interface accepts input from the user and converts it into Python code, which is then submitted to either *ABAQUS*®\Standard or *ABAQUS*®\Explicit. The code is then processed by one of these packages and the results are then returned to CAE for post-processing. Therefore, every job that is submitted has associated Python code, which may be edited by the user, by employing the "modify keywords" function in CAE. The automatically generated code was only edited to implement the UHYPER sub routines. Due to the length of the code and the minor changes that were made to it, no Python code is included here.

A.2 FORTRAN code

The FORTRAN code was written and compiled using the *Compaq*® FORTRAN compiler. Two UHYPER sub-routines were used - one based on the work of Delfino *et al* [24], the other taken directly from Koch [29]. As has been described in various sections of this work (chapters 2, 7.3, 4), the walls of arteries are multi-layered. Also, the mechanical properties of arteries vary

considerably throughout the body. In the case of the common vascular to vascular anastomois, the mechanical properties of the two biological sections will not match, even though they are both native to the body. Assuming that only the media and adventitia are modelled, four different materials will be present (a material each for the two medias and two adventitias). Even though the materials are different, their overall behaviour (hyperelastic) is the similar.

When modelling vascular tissue connections, the constants given by Koch [29] and Delfino *et al* [24] were modified to change the respective stiffnesses. The values from Delfino *et al* are $a = 44.2kPa$, $b = 16.7$. Those proposed by Koch are $C_{11} = 27.370kPa$, $C_{12} = 4.74$. The values given by Koch are for aortic valve leaflets, those by Delfino *et al* for the carotid artery.

When different sections were required, the same model (by Koch) was used, with the constants varying as shown below.

	C_{11}	$C_{12}(kPa)$
Media 1	8.35	44.2
Adventitia 1	4.74	27.37
Media 2	4.74	27.37
Adventitia 2	2.5	20

Table A.1: Constants used for the Multi-layered Arteries

Note that the increasing values of C_{11} and C_{12} are associated with higher stiffnesses. The media is stiffer than the adventitia and has been assigned constants accordingly. Graphs demonstrating the relationship between the two constants (C_{11} and C_{12}) from the work of Koch are given on the following page.

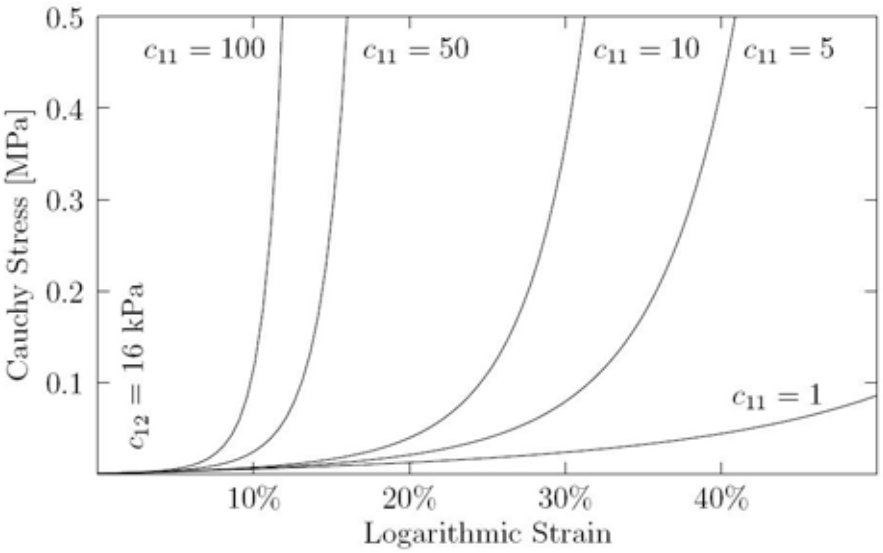

Figure A.1: Stress-strain plots
on the basis of the strain energy potential at constant $C_{12} = 16kPa$. The varying parameter C_{11} governs the transition behaviour from the initial compliant towards the stiff phase of the stress response [29].

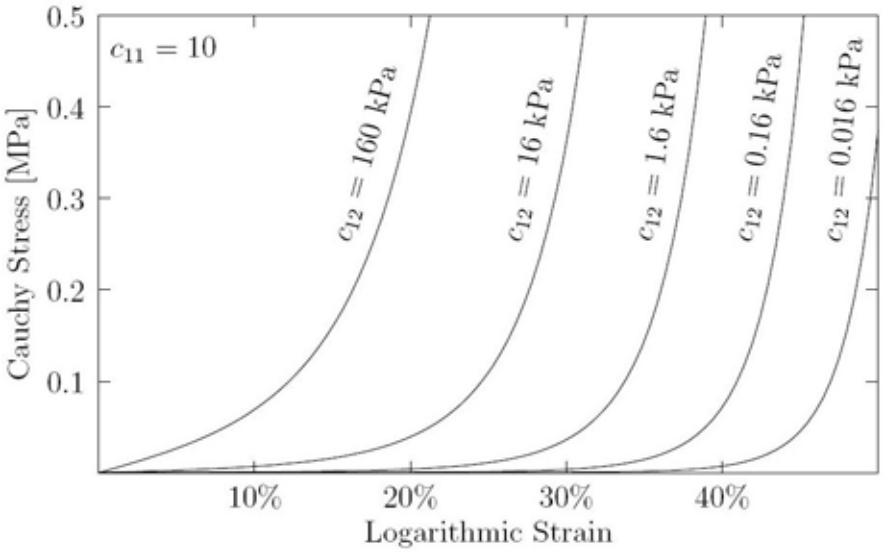

Figure A.2: Stress-strain plots
on the basis of the strain energy potential at constant $C_{11} = 10$. The varying parameter c12 defines the stress scale and as a result, the plots shift to the left for increasing C_{12} [29].

```
      SUBROUTINE UHYPER(BI1,BI2,AJ,U,UI1,UI2,UI3,TEMP,NOEL,CMNAME,
     $                  INCMPFLAG,NUMSTATEV,STATEV,NUMFIELDV,
     $                  FIELDV,FIELDVINC,NUMPROPS,PROPS)
C
      INCLUDE 'ABA_PARAM.INC'
C
      CHARACTER*80 CMNAME
      DIMENSION UI1(3),UI2(6),UI3(6),STATEV(*),FIELDV(*),
     $          FIELDVINC(*),PROPS(*)
C
      PARAMETER (ZERO=0.0D0,ONE=1.0D0, TWO=2.0D0, THREE=3.0D0)
C
      A = PROPS(1)
      B = PROPS(2)
C
C DEFINE THE STRAIN ENERGY FUNCTION AND ITS PARTIAL DERIVATIVES
C
      U=(A/B)*(EXP((B/TWO)*(BI3-THREE))-ONE)
      UI1(1)=(A/TWO)*EXP((B/TWO)*(BI3-THREE))
      UI2(1)=(A/TWO)*(B/TWO)*EXP((B/TWO)*(BI3-THREE))
C
C THE FOLLOWING PARTIAL DERIVATIVES ARE ALL ZERO.
C INCOMPRESSIBLE MATERIAL IMPLIES THAT BI3=0.
C
      UI1(2)=ZERO
      UI1(3)=ZERO
      UI2(2)=ZERO
      UI2(3)=ZERO
      UI2(4)=ZERO
      UI2(5)=ZERO
      UI2(6)=ZERO
      UI3(1)=ZERO
      UI3(2)=ZERO
      UI3(3)=ZERO
      UI3(4)=ZERO
      UI3(5)=ZERO
      UI3(6)=ZERO
      RETURN
      END
```

Figure A.3: UHYPER Subroutine Written Based on the Work of Delfino.

```
      SUBROUTINE UHYPER(BI1,BI2,AJ,U,UI1,UI2,UI3,TEMP,NOEL,CMNAME,
     $                  INCMPFLAG,NUMSTATEV,STATEV,NUMFIELDV,
     $                  FIELDV,FIELDVINC,NUMPROPS,PROPS)
C
      INCLUDE 'ABA_PARAM.INC'
C
      CHARACTER*80 CMNAME
      DIMENSION UI1(3),UI2(6),UI3(6),STATEV(*),FIELDV(*),
     $          FIELDVINC(*),PROPS(*)
C
      PARAMETER (ZERO=0.0D0,ONE=1.0D0, TWO=2.0D0, THREE=3.0D0)
C
      C1 = PROPS(1)
      C2 = PROPS(2)
C
C DEFINE STRAIN ENERGY FUNCTION AND ITS PARTIAL DERIVATIVES
C
      ETERM=(C2/TWO)*EXP(C1*(BI1-THREE))
      U=(ETERM-C2/TWO)/C1
      UI1(1)=ETERM
      UI2(1)=C1*ETERM
C
      UI1(2)=ZERO
      UI1(3)=ZERO
      UI2(2)=ZERO
      UI2(3)=ZERO
      UI2(4)=ZERO
      UI2(5)=ZERO
      UI2(6)=ZERO
      UI3(1)=ZERO
      UI3(2)=ZERO
      UI3(3)=ZERO
      UI3(4)=ZERO
      UI3(5)=ZERO
      UI3(6)=ZERO
      RETURN
      END
```

Figure A.4: Koch UHYPER Subroutine.

Appendix B

Evolution of the Model

B.1 Introduction

For anyone planning to continue with work similar to this, the evolution of the model described below will hopefully save hours and repetition.

B.2 Stitches

The stitches were originally modelled as analytical rigid components, including bell-shaped ends, to model the curving stitches. The analytical rigid components provided computationally inexpensive approximations, as they required no meshing. These stitches gave way to more sophisticated U-shaped discrete rigid parts. While these stitches model reality better than the analytical ones, they are far more expensive computationally due to the fine mesh that is required for the contact interactions. They also add an extra 658 elements each. For twelve stitches, that's an extra 7896 elements. The evolution of the stitches is shown on the following page.

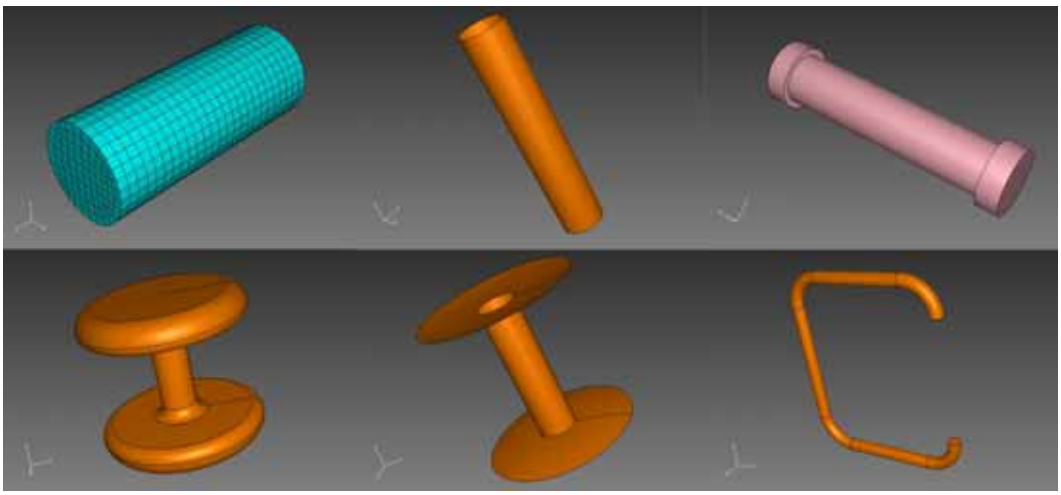

Figure B.1: Evolution of Stitches.
Top left shows a solid, deformable stitch. The others are rigid. All stitches were tested and discarded due to poor performance (computationally expensive or geometrically unsatisfactory).

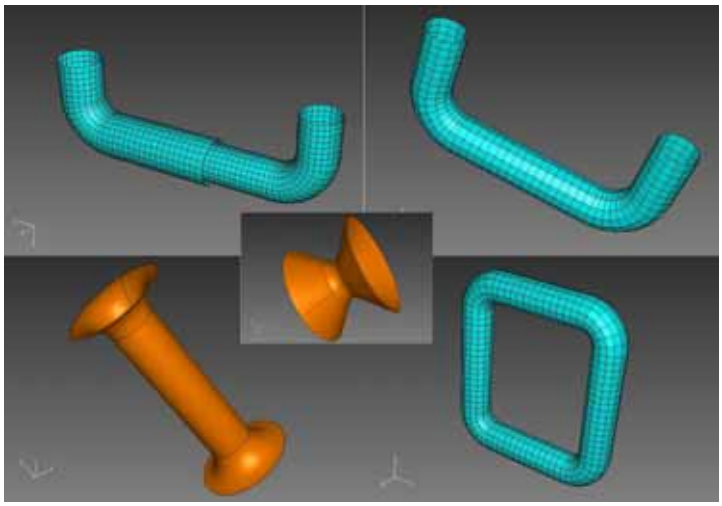

Figure B.2: Later evolution of Stitches.
Top left shows a rigid, two-part sliding stitch. Only the hoop and the U-shaped stitch were used in the final analyses.

B.3 Geometry

B.3.1 Various Configurations Attempted

Various geometrical configurations were modelled, with varying degrees of success. Most of the models were discarded due to the difficulties associated with pre-stressing the vascular sections (although attempts were made). The flanged connection shown below is not very realistic at all. In reality, the configuration would be substantially pre-stressed.

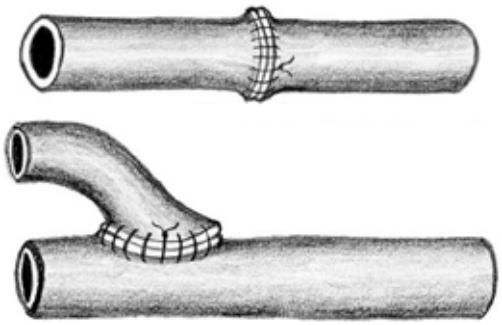

Figure B.3: Stitching configurations [10].

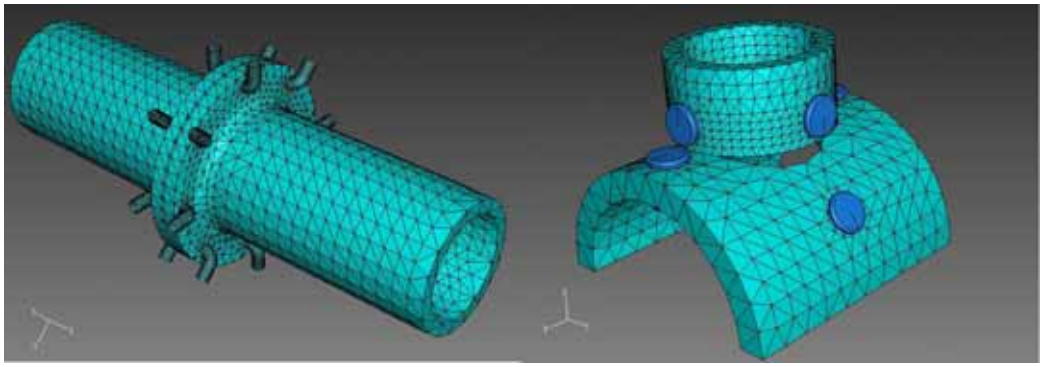

Figure B.4: Meshed assemblies of alternative configurations.

B.3.2 Various Refinements Investigated

In order to make the model as realistic as possible, several refinements were investigated.

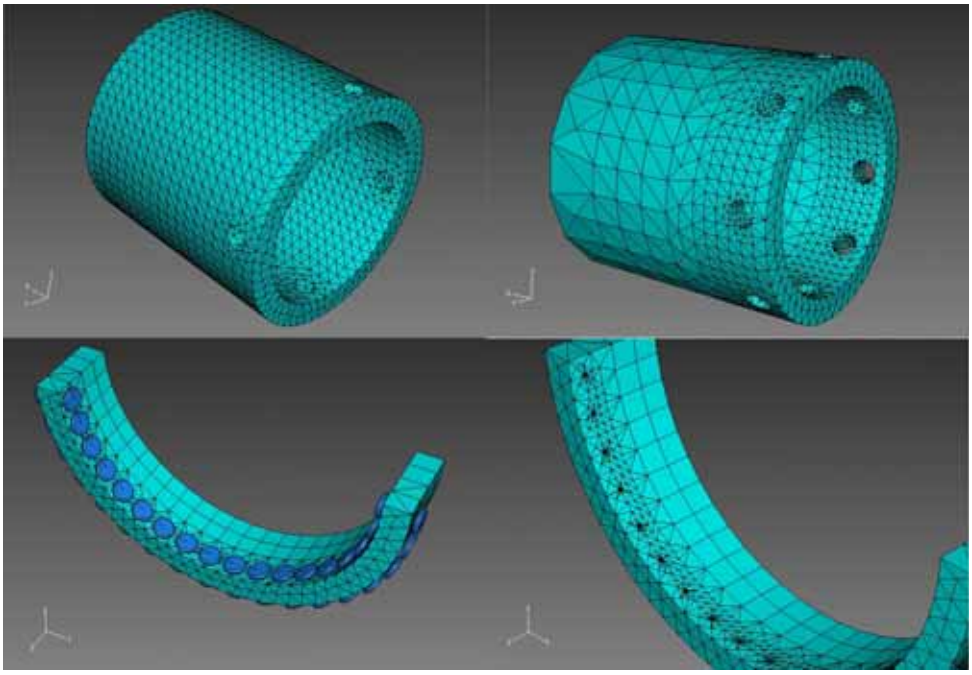

Figure B.5: Number of Stitches
The number of stitches was experimented with at length. First four, then eight, then sixteen and finally twelve. The four and eight stitch models were not refined enough, while the sixteen stitch model was much more computationally expensive for the small refinement that it offered.

Among the many refinements that were attempted, most were unsuitable due to computational complexity.

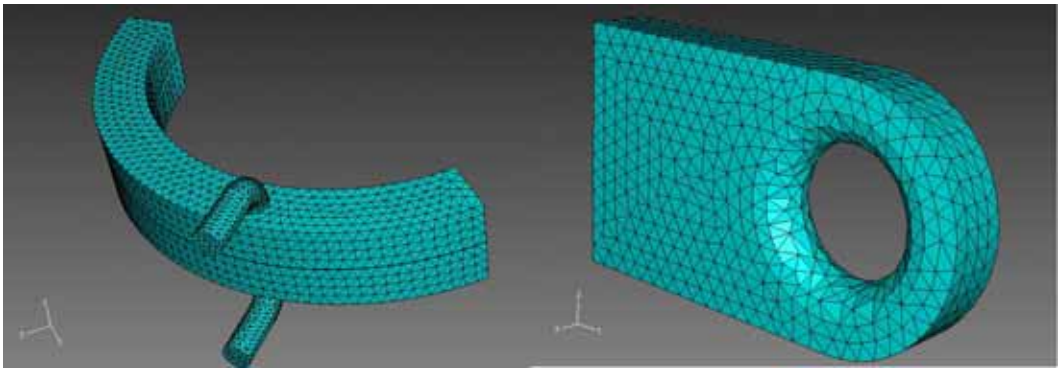

Figure B.6: Refinements
The stitching technique was deemed to be extremely important. The image on the left shows an attempt to model the stitches as three dimensional deformable components. The image on the right shows the complex meshing of fillets created on the stitch holes.

B.4 Material Model

Various material models were experimented with, both for the synthetic sections and the vascular sections. A latex model (Hyperelastic, Ogden, n=6) from the work of Yeoman [8] was extensively used. It was later discovered that solid-mechanically irrelevant sections of latex are used to seal the foam grafts. The work was therefore discarded.
For the material model, an initial approximation was made using a hyperelastic (Ogden, n=1) model proposed by Silver *et al* [15].
It was attempted to implement the model proposed by Saleeb *et al* [22], but all attempts failed.
Finally, a user-subroutine was written based on the work of Delfino *et al* [24] and another obtained from the work of Koch [29].

B.5 Loading

The pressure profiles are different for different parts of the body due to the damping that takes place, see chapter 2, "Biological Theory". The pulsatile loading *in vivo* was modelled in $ABAQUS^{®}$\Explicit by creating pressure profiles. A graph of the pressure versus time for one cycle was obtained from [30]. Using graphics editing software, a grid was superimposed onto the graph. The values of the pressure at multiple time intervals were recorded and tabulated. Using the "Amplitude" function in $ABAQUS^{®}$, the tabulated values were inserted to create the pulsatile loading. When $ABAQUS^{®}$ starts the step in which the load is applied, the pressure on the inside of the sections is zero. A smooth transition between the zero pressure state and the physiological pressures was created by ramping the pressure from zero to the minimum pressure in the cycle. The frequency of the cycle was set to 1Hz, equivalent to 60 beats per minute. The work was abandoned when it became necessary to implement a UHYPER and use spring elements.

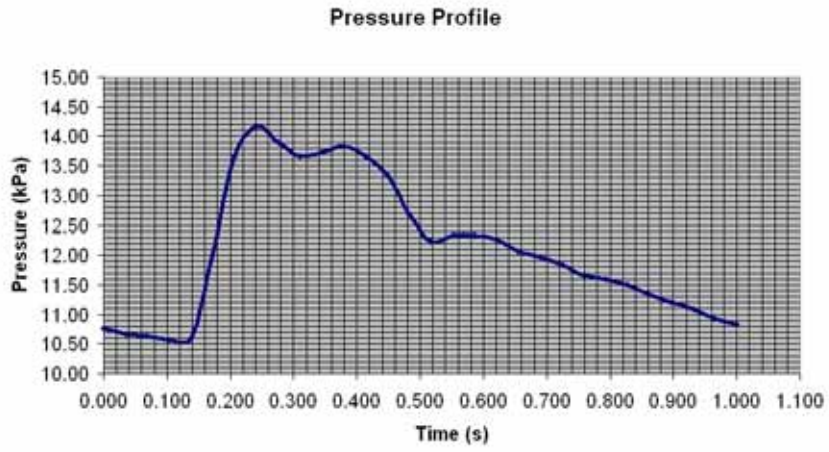

Figure B.7: Pulse profile

Appendix C

Interesting, but Obsolete Results

C.1 Introduction

Many of the preliminary jobs were run before certain major changes (improvements) were made to the simulations. These changes often made the numerical results obtained obsolete. However, not all of the analyses lost their worth. The results presented below should be viewed qualitatively, with the stress distributions and distortions being the most important factors.

C.2 Results

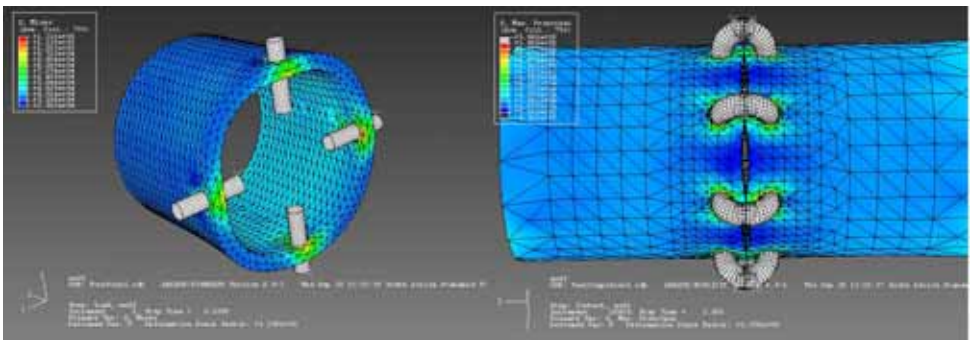

Figure C.1: Stress plots for four and eight stitch models
Note how the four stitch section adopts a rectangular shape when fully pressurised. The eight stitch model closely approximates the final configuration, as the stitches are 0.5mm in diameter.

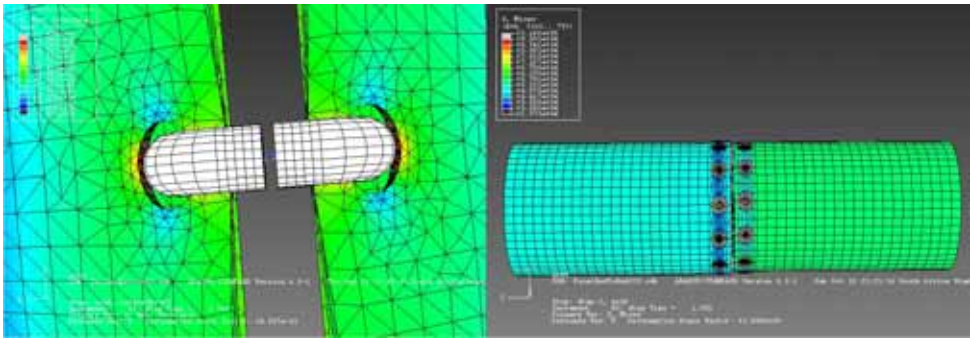

Figure C.2: Hole distortion and Longer Sections
The springs used to connect the two U-shaped stitches together were abandoned because they were not compatible with the desired pre-stressing. Section lengths twice the diameter were modelled, but made no significant difference to the results.

References

[1] M. Lemson, J. Tordoir, M. Daemen, and P. Kitslaar, "Intimal hyperplasia in vascular grafts," *Eur J Vasc Endovasc Surg*, vol. 19, pp. 336–350, 2000.

[2] G. Holzapfel, T. Gasser, and R. Ogden, "A new constitutive framework for arterial wall mechanics and a comparative study of material models," *Computational Biomechanics*, vol. 61, pp. 1–48, 2000.

[3] L. Sherwood, *Human Physiology - From Cells to Systems*, vol. 4. Brooks/Cole, 2001.

[4] F. Migliavacca and G. Dubini, "Computational modeling of vascular anastomoses," *Biomechan Model Mechanobiol*, vol. 3, pp. 235–250, 2005.

[5] "http://www.residentnet.com/running.htm," 26 October 2006.

[6] "http://www.residentnet.com/interupt.htm," 26 October 2006.

[7] "http://www.residentnet.com/purse.htm," 26 October 2006.

[8] M. Yeoman, *The Design and Optimisation of Fabric Reinforced Porous Prosthetic Grafts Using Finite Element Methods and Genetic Algorithms*. PhD thesis, University of Cape Town, 2004.

[9] "*abaqus*® user manual," vol. 6.5-1, 2004.

[10] P. Knez, K. Nelson, M. Hakimi, J. Al-Haidary, C. Schneider, and T. Schmitz-Rixen, "Rotational in vitro compliance measurement of diverse anastomotic configurations: a tool for anastomotic engineering," *Journal of Biomechanics*, vol. 37, pp. 275–280, 2004.

[11] Merriam-Webster, *Merriam-Webster's Medical Dictionary.* Merriam-Webster, Inc, 2002.

[12] *The American Heritage Dictionary of the English Language*, vol. Fourth Edition. Houghton Mifflin Company, 2000.

[13] *Collins Pocket Reference English Dictionary.* HarperCollins Publishers, 1993.

[14] J. Rhodin, *Handbook of Physiology, The Cardiovascular System*, vol. 2. Bethesda, Maryland: American Physiological Society, 1980.

[15] F. Silver, D. Christiansen, and C. Buntin, "Mechanical properties of the aorta: A review," *Critical Reviews in Biomed. Engr*, vol. 17, pp. 323–358, 1989.

[16] B. Young and J. Heath, *Functional Histology*, vol. 4. Churchill Livingstone, 2000.

[17] A. Kamiya and T. Togawa, "Adaptive regulation of wall shear stress to flow change in the canine carotid artery," *Am. J. Physiol.*, vol. 239, pp. H14–H21, 2001.

[18] M.Weston, K. Rhee, and J. Tarbell, "Compliance and diameter mismatch affect the wall shear rate distribution near an end-to-end anastomosis," *J. Biomechanics*, vol. 29, pp. 187–198, 1996.

[19] A. Noble, *The Cardiovascular System.* Elsevier Churchill Livingstone, First ed. 2005.

[20] W. Milnor, *Haemodynamics.* Baltimor: Williams and Wilkins, 1982.

[21] R. Shadwick, "Mechanical design in arteries," *The Journal of Experimental Biology*, vol. 202, pp. 3305–3315, 1999.

[22] A. Saleeb, D. Trowbridge, T. Wilt, J. Marks, and I. Vesely, "Dynamic pre-processing software for the hyperviscoelastic modeling of complex anisotropic biological tissue materials," *Advances in Engineering Software*, vol. 37, pp. 609–623, 2006.

[23] Y. Fung, *Biomechanics: Circulation*. New York: Springer-Verlag, 1984.

[24] A. Delfino, N. Stergiopulos, J. Moore, and J. Meister, "Residual strain effects on the stress field in a thick wall finite element model of the human carotid bifurcation," *J. Biomechanics*, vol. 30, pp. 777–786, 1997.

[25] G. Schajer, S. Green, A. Davis, and Y. Hsiang, "Influence of elastic nonlinearity on arterial anastomotic compliance," *Journal for Biomedical Engineering*, vol. 118, pp. 445–451, 1996.

[26] Y. Fung, K. Fronek, and P. Patitucci, "Pseudoelasticity of arteries and the choice of its mathematical expression," *American Journal of Physiology*, vol. 237, pp. H620–H631, 1979.

[27] A. Tiwari, K. Cheng, H. Salacinski, G. Hamilton, and A. Seifalian, "Improving the patency of vascular bypass grafts: the role of suture materials and surgical techniques on reducing anastomotic compliance mismatch," *Eur J Vasc Endovasc Surg*, vol. 25, pp. 287–295, 2003.

[28] M. Zidi and M. Cheref, "Mechanical analysis of a prototype of small diameter vascular prosthesis: numerical simulations," *Computers in Biology and Medicine*, vol. 33, pp. 65–75, 2003.

[29] T. Koch, "Non-linear finite element analyses of the aortic heart valve," Master's thesis, University of Cape Town, 2004.

[30] M. Hofer, G. Rappitsch, K. Perktold, W. Trubel, and H. Schima, "Numerical study of wall mechanics and fluid dynamics in end-to-side anastomoses and correlation to intimal hyperplasia," *J. Biomechanics*, vol. 29, pp. 1297–1308, 1996.